DOI: 10.1021/ic100905u

Inorganic Chemistry
Article

Synthesis, Structural Characterization, and Photophysical, Electrochemical, Intercomponent Energy-Transfer, and Anion-Sensing Studies of Imidazole 4,5-Bis(benzimidazole)-Bridged $Os^{II}Os^{II}$ and $Ru^{II}Os^{II}$ Bipyridine Complexes

Debasish Saha,[†] Shyamal Das,[†] Dinesh Maity,[†] Supriya Dutta,[‡] and Sujoy Baitalik*,[†]

[†]*Department of Chemistry, Inorganic Chemistry Section, Jadavpur University, Kolkata 700032, India, and*
[‡]*Department of Inorganic Chemistry, Indian Association for the Cultivation of Science, Kolkata 700 032, India*

Received May 7, 2010

Homo- and heterobimetallic complexes of composition $[(bpy)_2M^{II}(H_2Imbzim)M'^{II}(bpy)_2](ClO_4)_3 \cdot nH_2O$, where $M^{II} = M'^{II} = Os$ (**1**), $M^{II} = Ru$ and $M'^{II} = Os$ (**2**), $H_3Imbzim$ = 4,5-bis(benzimidazole-2-yl)imidazole, and bpy = 2,2′-bipyridine, have been synthesized and characterized using standard analytical and spectroscopic techniques. Both of the complexes crystallized in monoclinic form with the space group $P2_1/m$ for **1** and $P2_1/n$ for **2**. The absorption spectra, redox behavior, and luminescence properties of the complexes have been thoroughly investigated. The complexes display very intense, ligand-centered absorption bands in the UV region and moderately intense metal-to-ligand charge-transfer (MLCT) bands in the visible region. The bimetallic complexes show two successive one-electron reversible metal-centered oxidations. The strong fluorescence of free $H_3Imbzim$ is completely quenched in the metal complexes by energy transfer to the metal-based units, which exhibit their characteristic MLCT phosphorescence. The luminescence data of the heterometallic complex **2** show that electronic energy transfer takes place from the ruthenium center to the osmium-based component. The anion binding properties of the complexes have been studied in solutions using absorption, emission, and ^1H NMR spectral measurements. The metalloreceptors act as sensors for F^- and AcO^- ions. Sensing studies indicate the presence of two successive anion-induced deprotonation steps, leading to the formation of $[(bpy)_2M(HImbzim)M'(bpy)_2]^{2+}$ and $[(bpy)_2M(Imbzim)M'(bpy)_2]^{+}$ species. Double deprotonation is also observed in the presence of hydroxide. The binding affinities of different anions toward the receptors have been evaluated. Cyclic voltammetry measurements carried out in acetonitrile have provided evidence in favor of anion-dependent electrochemical responses of the bimetallic metalloreceptors with F^- and AcO^- ions.

Introduction

The supramolecular chemistry of anion recognition and binding is a subject of considerable contemporary research interest.[1−10] Anions being ubiquitous, quite a few of them play important roles in biological, aquatic, environmental, and industrial processes.[1−11] Consequently, lots of effort has been directed toward the design of receptors that can selectively recognize anions and act as sensors. A number of compounds containing urea, thiourea, amide, pyrrole, or imidazole subunits that are capable of providing hydrogen-bond-forming sites have been reported to exhibit strong affinity and selectivity toward certain anions.[1−9,12] With the purely organic hosts, attainment of the appropriate geometry can sometimes be problematic for proper host−guest interaction.[5] On the other

*To whom correspondence should be addressed: E-mail: sbaitalik@hotmail.com.

(1) (a) Sessler, J. L.; Gale, P. A.; Cho, W. S. *Anion Receptor Chemistry*; Royal Society of Chemistry: Cambridge, U.K., 2006. (b) *Supramolecular Chemistry of Anions*; Bianchi, A., Bowman-James, K., Garcia-Espańa, E., Eds.; Wiley-VCH: New York, 1997.
(2) Martínez-Máñez, R.; Sancenón, F. *Chem. Rev.* **2003**, *103*, 4419.
(3) (a) Peŕez, J.; Riera, L. *Chem. Commun.* **2008**, 533. (b) Peŕez, J.; Riera, L. *Chem. Soc. Rev.* **2008**, *37*, 2658.
(4) Steed, J. W. *Chem. Soc. Rev.* **2009**, *38*, 506.
(5) (a) Caltagirone, C.; Gale, P. A. *Chem. Soc. Rev.* **2009**, *38*, 520. (b) Gale, P. A.; Garcia-Garrido, S. E.; Garric, J. *Chem. Soc. Rev.* **2008**, *37*, 151. (c) Beer, P. D. *Chem. Commun.* **1996**, 689. (d) Beer, P. D.; Gale, P. A. *Angew. Chem., Int. Ed.* **2001**, *40*, 486. (e) Sessler, J. L.; Davis, J. M. *Acc. Chem. Res.* **2001**, *34*, 989.
(6) (a) Amendola, V.; Fabbrizzi, L. *Chem. Commun.* **2009**, 513. (b) Amendola, V.; Gómez, E. D.; Fabbrizzi, L.; Licchelli, M. *Acc. Chem. Res.* **2006**, *39*, 343.
(7) (a) dos Santos, C. M. G.; Harte, A. J.; Quinn, S. T.; Gunnlaugsson, T. *Coord. Chem. Rev.* **2008**, *252*, 2512. (b) Gunnlaugsson, T.; Glynn, M.; Tocci (nee Hussey), G. M.; Kruger, P. E.; Pfeffer, F. M. *Coord. Chem. Rev.* **2006**, *250*, 3094.
(8) Rice, C. R. *Coord. Chem. Rev.* **2006**, *250*, 3190.
(9) (a) Bowman-James, K. *Acc. Chem. Res.* **2005**, *38*, 671. (b) Sun, S.-S.; Lees, A. J. *Coord. Chem. Rev.* **2002**, *230*, 171. (c) Bondy, C. R.; Loeb, S. J. *Coord. Chem. Rev.* **2003**, *240*, 77. (d) Suksai, C.; Tuntulani, T. *Top. Curr. Chem.* **2005**, *255*, 163. (e) de Silva, A. P.; Gunaratne, H. Q. N.; Gunnlaugsson, T.; Huxley, A. J. M.; McCoy, C. P.; Rademacher, J. T.; Rice, T. E. *Chem. Rev.* **1997**, *97*, 1515.
(10) (a) Lam, S.-T.; Zhu, N.; Yam, V. W. W. *Inorg. Chem.* **2009**, *48*, 9664. (b) Wong, K. M. C.; Tang, W. S.; Lu, X. X.; Zhu, N.; Yam, V. W. W. *Inorg. Chem.* **2005**, *44*, 1492. (c) Yam, V. W. W.; Ko, C. C.; Zhu, N. *J. Am. Chem. Soc.* **2004**, *126*, 12734. (d) Yam, V. W. W. *Acc. Chem. Res.* **2002**, *35*, 555.
(11) Schraderr, T., Hamilton, A. D., Eds. *Functional Synthetic Receptors*; Wiley-VCH: Weinheim, Germany, 2005.

Published on Web 11/29/2010

hand, metal ions can profitably orient the ligands in the right conformations so that their hydrogen-bond-donor groups can converge toward an external guest.[2−4] As part of our interest in exploring new receptors for anions, we have sought to examine 4,5-bis(benzimidazole-2-yl)imidazole (H_3Imbzim) as a potential motif for anion sensing. H_3Imbzim contains three imidazole NH protons, which could be donated for hydrogen bonding to the anions. It should be noted, however, that the acid dissociation constant of the hydrogen atom that participates in the hydrogen-bond formation with the anionic analyte is important because in some cases it may be problematic to differentiate whether hydrogen-bond formation with the anions has occurred or proton transfer to the basic anion has taken place.[5,6,13] Clearly, factors such as the acidity of the receptor, basicity of the anion, and stability of the conjugate base, all of which are solvent-dependent, control the overall process.

In recent years, the development of triple-channel sensors, that is, sensors where interaction can be sensed by monitoring three different physicochemical outputs, has emerged as a topic of intensive studies.[2−5] Inasmuch as ruthenium(II) polypyridine complexes are known to display unique photophysical and redox properties and are considered as ionic building blocks for the design of photomolecular devices,[14,15] a number of ruthenium(II) polypyridine based receptors have been designed as ion sensors,[2−4,16−26] although such sensors for anions are relatively few. Compared to the ruthenium(II) systems, studies made for analogous osmium(II) compounds, and particularly heterometallic ruthenium(II)−osmium(II) complexes are extremely rare.[2,18,19b] In the heterometallic ruthenium(II)−osmium(II) complex, photoinduced energy transfer from the ruthenium-based unit to the osmium-based unit is also expected to take place. In our endeavor to develop triple-channel anion sensors, we have studied in detail the structural, spectroscopic, and physicochemical properties of mixed-ligand homobimetallic osmium(II) and heterobimetallic ruthenium(II)−osmium(II) complexes derived from 2,2′-bipyridine (bpy) and 4,5-bis(benzimidazole-2-yl)imidazole (H_3Imbzim) ligands and their interactions with several anions, including F^- and AcO^-. To our knowledge, no such studies have been reported in the literature for $[(bpy)_2Os^{II}(H_2Imbzim)Os^{II}(bpy)_2]^{3+}$ and $[(bpy)_2Ru^{II}(H_2Imbzim)\,Os^{II}(bpy)_2]^{3+}$ systems. H_3Imbzim is a bifunctional molecule, possessing both the lone electron pairs that can be coordinated to $M^{II}(bpy)_2$ (M = Ru and Os) fragments as a first-coordination sphere and the imidazole NH protons in the second-coordination sphere, which may donate hydrogen bonds to the anions. As will be seen, consequent to anion interaction, remarkable changes in color that can be followed by naked eyes and similar photoluminescence and electrochemical responses occur.

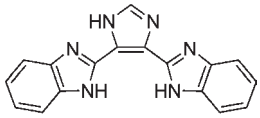

H_3Imbzim

Experimental Section

Materials. Reagent-grade chemicals obtained from commercial sources were used as received. Solvents were purified and dried according to standard methods.[27] Imidazole-4,5-dicarboxylic acid, *o*-phenylenediamine, and tetrabutylammonium (TBA) salt of the anions were purchased from Sigma−Aldrich. The bridging 4,5-bis(benzimidazolyl)imidazole (H_3Imbzim) ligand and $[(bpy)_2Ru(H_3Imbzim)](ClO_4)_2\cdot 2H_2O$ were prepared according to the literature method published by us.[19a] *cis*-$[Ru(bpy)_2Cl_2]\cdot 2H_2O$[28] and *cis*-$[Os(bpy)_2Cl_2]$[29] were prepared by the literature method. $AgClO_4$ was prepared from silver carbonate and perchloric acid and recrystallized from benzene.

Preparation of the Metal Complexes. The complexes were prepared under oxygen and moisture-free dinitrogen using standard Schlenk techniques.

Caution! *$AgClO_4$ and perchlorate salts of the metal complexes used in this study are potentially explosive and therefore should be handled with care in small quantities.*

(12) (a) Gunnlaugsson, T.; Stomeo, F. *Org. Biomol. Chem.* **2007**, *5*, 1999. (b) Leonard, J. P.; Nolan, C. B.; Stomeo, F.; Gunnlaugsson, T. *Top. Curr. Chem.* **2007**, *281*, 1. (c) Mizukami, S.; Nagano, T.; Urano, Y.; Odani, A.; Kikuchi, K. *J. Am. Chem. Soc.* **2002**, *124*, 3902. (d) Cho, E. J.; Moon, J. W.; Ko, S. W.; Lee, J. Y.; Kim, S. K.; Yoon, J.; Nam, K. C. *J. Am. Chem. Soc.* **2003**, *125*, 12376. (e) Otón, F.; Tárraga, A.; Espinosa, A.; Velasco, M. D.; Molina, P. *J. Org. Chem.* **2006**, *71*, 4590. (f) Lin, T.-P.; Chen, C.-Y.; Wen, Y.-S.; Sun, S.-S. *Inorg. Chem.* **2007**, *46*, 9201. (g) Sun, S.-S.; Lees, A. J.; Zavalij, P. Y. *Inorg. Chem.* **2003**, *42*, 3445. (h) Wu, C.-Y.; Chen, M.-S.; Lin, C.-A.; Lin, S.-C.; Sun, S.-S. *Chem.—Eur. J.* **2006**, *12*, 2263.

(13) Steiner, T. *Angew. Chem., Int. Ed.* **2001**, *41*, 48.

(14) (a) Juris, A.; Balzani, V.; Barigelletti, F.; Campagna, S.; Belser, P.; von Zelewsky, A. *Coord. Chem. Rev.* **1988**, *84*, 85. (b) Meyer, T. J. *Pure Appl. Chem.* **1986**, *58*, 1193. (c) Balzani, V.; Juris, A.; Venturi, M. *Chem. Rev.* **1996**, *96*, 759. (d) Baba, A. I.; Shaw, J. R.; Simon, J. A.; Thummel, R. P.; Schmehl, R. H. *Coord. Chem. Rev.* **1998**, *171*, 43. (e) Medlycott, E. A.; Hanan, G. S. *Coord. Chem. Rev.* **2006**, *250*, 1763. (f) Kalyanasundaram, K. *Photochemistry of Polypyridine and Porphyrin Complexes*; Academic Press: London, 1992. (g) Sauvage, J.-P.; Collin, J.-P.; Chambron, J.-C.; Guillerez, S.; Coudret, C.; Balzani, V.; Barigelletti, F.; De Cola, L.; Flamigni, L. *Chem. Rev.* **1994**, *94*, 993. (h) Giuffrida, G.; Campagna, S. *Coord. Chem. Rev.* **1994**, *135*/*136*, 517.

(15) (a) Baitalik, S.; Wang, X.; Schmehl, R. H. *J. Am. Chem. Soc.* **2004**, *126*, 16304. (b) Wang, X.; Del Guerzo, A.; Baitalik, S.; Simon, G.; Shaw, G. B.; Chen., L. X.; Schmehl, R. H. *Photosynth. Res.* **2006**, *87*, 83. (c) Baitalik, S.; Flörke, U.; Nag, K. *Inorg. Chem.* **1999**, *38*, 3296.

(16) Anzebacher, P.; Tyson, D. S.; Jurslkova, K.; Castellano, F. N. *J. Am. Chem. Soc.* **2002**, *124*, 6232.

(17) Mizuno, T.; Wei, W.-H.; Eller, L. R.; Sessler, J. L. *J. Am. Chem. Soc.* **2002**, *124*, 1134.

(18) (a) Beer, P. D.; Szemes, F.; Balzani, V.; Salà, C. M.; Drew, M. G. B.; Dent, S. W.; Maestri, M. *J. Am. Chem. Soc.* **1997**, *119*, 11864. (b) Szemes, F.; Hesek, D.; Chen, Z.; Dent, S. W.; Drew, M. G. B.; Goulden, A. J.; Graydon, A. R.; Grieve, A.; Mortimer, R. J.; Wear, T. J.; Weightman, J. S.; Beer, P. D. *Inorg. Chem.* **1996**, *35*, 5868.

(19) (a) Saha, D.; Das, S.; Bhaumik, C.; Dutta, S.; Baitalik, S. *Inorg. Chem.* **2010**, *49*, 2334. (b) Das, S.; Saha, D.; Bhaumik, C.; Dutta, S.; Baitalik, S. *Dalton Trans.* **2010**, *39*, 4162. (c) Bhaumik, C.; Das, S.; Saha, D.; Dutta, S.; Baitalik, S. *Inorg. Chem.* **2010**, *49*, 5049.

(20) (a) Cui, Y.; Mo, H.-J.; Chen, J.-C.; Niu, Y.-L.; Zhong, Y.-R.; Zheng, K.-C.; Ye, B.-H. *Inorg. Chem.* **2007**, *46*, 6427. (b) Cui, Y.; Niu, Y.-L.; Cao, M. L.; Wang, K.; Mo, H.-J.; Zhong, Y.-R.; Ye, B.-H. *Inorg. Chem.* **2008**, *47*, 5616.

(21) (a) Lin, Z.-H.; Ou, S.-J.; Duan, C.-Y.; Zhang, B.-G.; Bai, Z.-P. *Chem. Commun.* **2006**, 624. (b) Lin, Z.-H.; Zhao, Y.-G.; Duan, C.-Y.; Zhang, B.-G.; Bai, Z.-P. *Dalton Trans.* **2006**, 3678.

(22) Ion, L.; Morales, D.; Perez, J.; Riera, L.; Riera, V.; Kowenicki, R. A.; McPartlin, M. *Chem. Commun.* **2006**, 91.

(23) Zapata, F.; Caballero, A.; Espinosa, A.; Tárraga, A.; Molina, P. *J. Org. Chem.* **2008**, *73*, 4034.

(24) Jose, D. A.; Kar, P.; Koley, D.; Ganguly, B.; Thiel, W.; Ghosh, H. N.; Das, A. *Inorg. Chem.* **2007**, *46*, 5576.

(25) Watanabe, S.; Onogawa, O.; Komatsu, Y.; Yoshida, K. *J. Am. Chem. Soc.* **1998**, *120*, 229.

(26) Aoki, S.; Zulkefeli, M.; Shiro, M.; Kohsako, M.; Takeda, K.; Kimura, E. *J. Am. Chem. Soc.* **2005**, *127*, 9129.

(27) Perrin, D. D.; Armarego, W. L.; Perrin, D. R. *Purification of Laboratory Chemicals*, 2nd ed.; Pergamon: Oxford, U.K., 1980.

(28) Sullivan, B. P.; Meyer, T. J. *Inorg. Chem.* **1978**, *17*, 3334.

(29) Lay, P. A.; Sargeson, A. M.; Taube, H. *Inorg. Synth.* **1986**, *24*, 291.

$[(bpy)_2Os(H_2Imbzim)Os(bpy)_2](ClO_4)_3\cdot H_2O$ (1). A mixture of *cis*-$[Os(bpy)_2Cl_2]$ (0.57 g, 1 mmol), $H_3Imbzim$ (0.15 g, 0.5 mmol), and triethylamine (0.05 g, 0.5 mmol) in ethanol−water (1:1, 100 mL) was heated under reflux with continuous stirring for 72 h. The solution was filtered, and to the cooled filtrate (ca. 5 °C) was added an aqueous solution (5 mL) of $NaClO_4\cdot H_2O$ (1 g). After stirring for 10 min, the dark shiny microcrystalline compound that deposited was filtered. The product was recrystallized twice from methanol−water (10:1) containing a few drops of 10^{-4} M $HClO_4$. Yield: 0.37 g (46%). Anal. Calcd for $C_{57}H_{45}Cl_3N_{14}O_{13}Os_2$: C, 42.24; H, 2.80; N, 12.10. Found: C, 42.21; H, 2.81; N, 12.08. ^{1}H NMR {300 MHz, DMSO-d_6, δ (ppm)}: 13.70 (s, 2H, NH benzimidazole), 8.80 (d, 2H, J = 8.0 Hz, H3), 8.76 (d, 2H, J = 8.1 Hz, H3), 8.71 (d, 2H, J = 8.0 Hz, H3), 8.64 (d, 2H, J = 7.9 Hz, H3), 8.58 (d, 2H, J = 5.3 Hz, H6), 8.02−7.65 (m, 10H, 8H4 + 2H6), 7.60−7.56 (m, 4H, 2H6 + 2H11), 7.46 (t, 2H, J = 6.6 Hz, H5), 7.36−7.33 (m, 4H, 2H5 + 2H6), 7.24 (t, 2H, J = 6.4 Hz, H5), 7.06 (t, 2H, J = 6.1 Hz, H5), 6.99 (t, 2H, J = 7.8 Hz, H12), 6.86 (t, 2H, J = 7.8 Hz, H13), 5.64 (d, 2H, J = 8.2 Hz, H14), 5.15 (s, 1H, H7). ESI-MS (positive, CH_3CN): m/z 434.98 (12%) $[(bpy)_2Os(H_2Imbzim)Os(bpy)_2]^{3+}$; 651.95 (100%) $[(bpy)_2Os(HImbzim)Os(bpy)_2]^{2+}$. UV−vis [$CH_2Cl_2$; λ_{max}, nm (ε, M^{-1} cm^{-1})]: 705 br (4370), 638 br (5120), 505 (21 550), 462 (22 200), 417 (24 700), 363 (35 900), 342 (31 000), 292 (98 200), 245 (60 700).

$[(bpy)_2Ru(H_2Imbzim)Os(bpy)_2](ClO_4)_3\cdot 2H_2O$ (2). An ethanol−water (1:1) solution (150 mL) of $[(bpy)_2Ru(H_3Imbzim)](ClO_4)_2\cdot 2H_2O$ (0.47 g. 0.5 mmol) was treated with $[Os(bpy)_2Cl_2]$ (0.29 g, 0.51 mmol), followed by triethylamine (0.05 g, 0.5 mmol). The mixture was heated under reflux with continuous stirring for 48 h, after which it was filtered hot. To the filtrate was added an aqueous solution (5 mL) of $NaClO_4\cdot H_2O$ (1 g), and the resulting solution was rotary-evaporated to ca. 50 mL and then cooled to −5 °C for 10 h. The dark microcrystalline product that deposited was collected by filtration and recrystallized from methanol−water (10:1) containing a few drops of 10^{-4} M $HClO_4$. Yield: 0.45 g (58%). Anal. Calcd for $C_{57}H_{47}Cl_3N_{14}O_{14}OsRu$: C, 44.18; H, 3.05; N, 12.65. Found: C, 44.15; H, 3.06; N, 12.63. ^{1}H NMR {300 MHz, DMSO-d_6, δ (ppm)}: 13.65 (s, 1H, NH benzimidazole), 13.58 (s, 1H, NH benzimidazole), 8.84−8.65 (m, nr, 8H, H3), 8.42 (d, nr, 2H, H6), 8.29 (m, br, 1H, H4), 8.19 (td, 1H, H4), 8.07−7.94 (m, nr, 6H, 4H4 + 2H6), 7.83−7.76 (m, nr, 4H, 2H4 + 2H6), 7.64 (m, 2H, H11 + H11′), 7.70−7.40 (m, nr, 4H, H5), 7.39−7.25 (m, nr, 4H, H5), 7.18−7.06 (m, nr, 4H, 2H6 + H12 + H12′), 6.98 (m, nr, 2H, H13 + H13′), 5.72 (s, 1H, H7), 5.55 (nr, 1H, H14′), 5.04 (nr, 1H, H14). ESI-MS (positive, CH_3CN): m/z 404.98 (6%) $[(bpy)_2Ru(H_2Imbzim)Os(bpy)_2]^{3+}$; 606.96 (100%) $[(bpy)_2Ru(HImbzim)Os(bpy)_2]^{2+}$; 657.39 (5%) $[(bpy)_2Ru(H_2Imbzim)Os(bpy)_2(ClO_4)]^{2+}$, 1313.78 (5%) $[(bpy)_2Ru(HImbzim)Os(bpy)_2(ClO_4)_2]^{+}$, 1414.30 (5%) $[(bpy)_2Ru(H_2Imbzim)Os(bpy)_2(ClO_4)_2]^{+}$. UV−vis [$CH_2Cl_2$; λ_{max}, nm (ε, M^{-1} cm^{-1})]: 705 br (2500), 637 br (2900), 485 (27 600), 451 (29 400), 392 (32 000), 358 (51 600), 340 (44 700), 292 (112 600), 245 (82 100).

Physical Measurements. Elemental (C, H, and N) analyses were performed on a Perkin-Elmer 2400II analyzer. Electrospray ionization mass spectra (ESI-MS) were obtained on a Micromass Qtof YA 263 mass spectrometer. ^{1}H and $\{^1H-^1H\}$ COSY spectra were obtained on a Bruker Avance DPX 300 spectrometer using DMSO-d_6 solutions. For a typical titration experiment, 3 μL aliquots of a TBA salt of the anion (0.2 M in DMSO-d_6) were added to a DMSO-d_6 solution of the complexes (2.5×10^{-3} M).

Electronic absorption spectra were obtained with a Shimadzu UV 1800 spectrophotometer at room temperature. For a typical titration experiment, 4 μL aliquots of a TBA salts of F^-, Cl^-, Br^-, I^-, AcO^-, and HSO_4^- (4.0×10^{-3} M in acetonitrile) were added to a 2.5 mL solution of the complexes (2.0×10^{-5} M in acetonitrile). The binding constants were evaluated from the absorbance data using eq 1.[30]

$$A_{obs} = (A_0 + A_\infty K[G]_T)/(1 + K[G]_T) \quad (1)$$

where A_{obs} is the observed absorbance, A_0 is the absorbance of the free receptor, A_∞ is the maximum absorbance induced by the presence of a given anionic guest, $[G]_T$ is the total concentration of the guest, and K is the binding constant of the host−guest entity. Binding constants were performed in duplicate, and the average value is reported.

Emission spectra were recorded on a Perkin-Elmer LS55 fluorescence spectrophotometer. The room temperature spectra were obtained in acetonitrile or dichloromethane solutions, while the spectra at 77 K were recorded in a 4:1 ethanol−methanol glass. Photoluminescence titrations were carried out with the same sets of solutions as those made with spectrophotometry. Quantum yields were determined by a relative method using $[Ru(bpy)_3]^{2+}$ in the same solvent as the standard.[31] The quantum yields were calculated by using eq 2.

$$\Phi_r = \Phi_{std}\frac{A_{std}}{A_r}\frac{I_r}{I_{std}}\frac{{\eta_r}^2}{{\eta_{std}}^2} \quad (2)$$

where Φ_r and Φ_{std} are the quantum yields of unknown and standard samples [Φ_{std} = 0.089 (at 298 K) and 0.35 (at 77 K) in ethanol−methanol (4:1) at λ_{ex} = 450 nm], A_r and A_{std} (< 0.1) are the solution absorbances at the excitation wavelength (λ_{ex}), I_r and I_{std} are the integrated emission intensities, and η_r and η_{std} are the refractive indices of the solvent.[31]

Time-correlated single-photon-counting (TCSPC) measurements were carried out for the luminescence decay of complexes in a dichloromethane solution at room temperature. For TCSPC measurement, the photoexcitation was made at 440 nm using a picosecond diode laser (IBH Nanoled-07) in an IBH Fluorocube apparatus. The fluorescence decay data were collected on a Hamamatsu MCP photomultiplier (R3809) and were analyzed by using IBH DAS6 software.

The electrochemical measurements were carried out with a BAS 100B electrochemistry system. A three-electrode assembly comprising a platinum (for oxidation) or glassy carbon (for reduction) working electrode, a platinum auxiliary electrode, and an aqueous Ag/AgCl reference electrode were used. The cyclic voltammetry (CV) and square-wave voltammetry (SWV) measurements were carried out at 25 °C in an acetonitrile solution of the complexes (ca. 1 mM), and the concentration of the supporting electrolyte tetraethylammonium perchlorate was maintained at 0.1 M. All of the potentials reported in this study were referenced against the Ag/AgCl electrode, which under the given experimental conditions gave a value of 0.36 V for the ferrocene/ferrocenium couple. For electrochemical titrations, 25 μL aliquots of TBA salts of the anions (4.0×10^{-2} M in acetonitrile) were added to a 5 mL (1.0×10^{-3} M) solution of receptors in acetonitrile.

Experimental uncertainties were as follows: absorption maxima, ±2 nm; molar absorption coefficients, 10%; emission maxima, ±5 nm; excited-state lifetimes, 10%; luminescence quantum yields, 20%; redox potentials, ±10 mV.

X-ray Crystal Structure Determination. Diffraction-quality crystals of **1** were obtained by diffusing toluene to a dichloromethane−acetonitrile (2:1) solution. In the case of **2**, diethyl ether was layered over an acetonitrile solution of **2**. X-ray diffraction data for both of the crystals mounted on a glass fiber and coated with perfluoropolyether oil were collected on a

(30) Schneider, H.-J.; Yatsimirsky, A. *Principles and Methods in Supramolecular Chemistry*; John Wiley and Sons: London, 2000; p 142.

(31) (a) Nakamaru, K. *Bull. Chem. Soc. Jpn.* **1982**, *55*, 1639 and references cited therein. (b) Demas, J. N.; Crosby, G. A. *J. Am. Chem. Soc.* **1971**, *93*, 2841. (c) van Houten, J.; Watts, R. J. *J. Am. Chem. Soc.* **1976**, *98*, 4853.

Table 1. Crystallographic Data for **1** and **2**

	1	**2**
formula	$C_{59}H_{47}Cl_7N_{14}O_{13}Os_2$	$C_{57}H_{43}Cl_3N_{14}O_{12}OsRu$
fw	1788.66	1513.67
T (K)	120(2)	120(2)
cryst syst	monoclinic	monoclinic
space group	$P2_1/m$	$P2_1/n$
a (Å)	12.5661(7)	12.4677(6)
b (Å)	20.3194(12)	21.8071(11)
c (Å)	12.8467(7)	23.6161(12)
α (deg)	90.00	90.00
β (deg)	91.886(2)	90.206(2)
γ (deg)	90.00	90.00
V (Å^3)	3278.4(3)	6420.8(6)
D_c (g cm^{-3})	1.812	1.566
Z	2	4
μ (mm^{-1})	4.231	2.406
F(000)	1748	3000
θ range (deg)	2.45−27.50	1.27−25.06
data/restraints/params	7710/0/419	11 348/0/789
GOF on F^2	1.24	1.16
R1[a] [$I > 2\sigma(I)$], wR2[b] (all data)	0.0619, 0.2174	0.0726, 0.2090
$\Delta\rho_{max}/\Delta\rho_{min}$ (e Å^{-1})	3.55/−1.37	3.83/−1.28

[a] $R1(F) = [\sum||F_o| - |F_c||/\sum|F_o|]$. [b] $wR2(F^2) = [\sum w(F_o^2 - F_c^2)^2/\sum w(F_o^2)^2]^{1/2}$.

Bruker AXS SMART APEX II diffractometer at 120 K equipped with a CCD detector using graphite-monochromated Mo Kα radiation (λ = 0.710 73 Å). Crystallographic data and details of the structure determination are summarized in Table 1. The data were processed with *SAINT*,[32] and absorption corrections were made with *SADABS*.[32] The structure was solved by direct and Fourier methods and refined by full-matrix least squares based on F^2 using the *WINGX* software, which utilizes *SHELX-97*.[33] For structure solution and refinement, the *SHELXTL* software package[34] was used. The non-hydrogen atoms were refined anisotropically, while the hydrogen atoms were placed with fixed thermal parameters at idealized positions. In the case of **1**, the C9, C22, C23, C24, O2, and O3 atoms have been refined isotropically. Further, in the complex cation $\mathbf{2}^{3+}$, both of the metal sites are disordered over two sites with almost equal occupancy (0.5 Ru/0.5 Os for each metal center). For both compounds, their electron density maps showed the presence of some unassignable peaks, which were removed by running the program *SQUEEZE*.[35] The final least-squares refinement [$I > 200\sigma(I)$] converged to reasonably good R values: R1 = 0.0619 (7710), wR2 = 0.2174 (7710) for **1** and R1 = 0.0726, (11 348), wR2 = 0.2090 (11 348) for **2**.

CCDC reference numbers are 775880 for **1** and 775881 for **2**.

Results and Discussion

Synthesis. Synthesis of the ligand H_3Imbzim and the monometallic ruthenium(II) complex $[(bpy)_2Ru(H_3Imbzim)](ClO_4)_2\cdot 2H_2O$ was undertaken by the following methods previously described.[19a] The reaction between *cis*-$[(bpy)_2OsCl_2]$ and H_3Imbzim, leading to the substitution of two chloride ions by the two imine nitrogen donors of the incoming ligand, is kinetically slow. Thus, the symmetrical bimetallic osmium(II) complex **1** has been obtained by treating a mixture of *cis*-$[(bpy)_2OsCl_2]$, H_3Imbzim, and triethylamine in a 2:1:1 molar ratio in boiling ethanol−water (1:1) for 72 h. The heterobimetallic complex **2** was produced by treating equimolar amounts of $[(bpy)_2Ru(H_3Imbzim)](ClO_4)_2\cdot 2H_2O$, $[(bpy)_2OsCl_2]$, and triethylamine in ethanol−water at its boiling temperature for 48 h. The complexes initially isolated as mixtures of diastereoisomers were separated by fractional recrystallization from a MeOH−CH_3CN (2:1) mixture.

The compounds have been characterized by their elemental (C, H, and N) analyses, ESI-MS, UV−vis, and ^{1}H NMR spectroscopic measurements, and the results are given in the Experimental Section. ESI-MS of the heterobimetallic compound **2** was of particular interest because the X-ray structure determination of **2** revealed that the two metal centers in this compound are positionally disordered over two sites with equal occupancy. ESI-MS of **2** (Figure S1, Supporting Information) shows a strong clusters of peaks with m/z 606.96, which correspond to those of $[(bpy)_2Ru(HImbzim)Os(bpy)_2]^{2+}$. The excellent agreement between the observed and simulated isotopic distribution patterns of the peak clearly indicates that **2** is a genuine heterobimetallic $Ru^{II}Os^{II}$ compound and is not a 1:1 stoichiometric combination of the homodinuclear $Os^{II}Os^{II}$ and $Ru^{II}Ru^{II}$ compounds. Thus, the possibility of static disorder is ruled out.

Description of the Crystal Structures of 1 and 2. ORTEP representations of the $\mathbf{1}^{3+}$ and $\mathbf{2}^{3+}$ cations along with their atom labels are shown in parts a and b of Figure 1, respectively. Selected bond distances and angles of **1** and **2** are given in Table 2. In terms of chirality descriptors, homodinuclear $\mathbf{1}^{3+}$ is of the meso (ΛΔ) form, while heterodinuclear $\mathbf{2}^{3+}$ is a ΛΔ/ΔΛ enantiomeric pair. The structure of *meso*-$[(bpy)_2Ru(H_2Imzbzim)Ru(bpy)_2](ClO_4)_3\cdot CH_2Cl_2$ was reported previously.[19a] However, some of its structural aspects that are relevant to this study and were not considered earlier will be discussed here. In $\mathbf{1}^{3+}$, each of the two osmium centers is coordinated by one $Os^{II}(bpy)_2$ unit of each half of the bridging $H_2Imbzim^-$ ligand and the two osmium(II) centers are bridged by one imidazolate nitrogen N3 and one benzimidazole nitrogen N1, while in $\mathbf{2}^{3+}$, the two $M^{II}(bpy)_2$ units are bridged by the imidazolate nitrogen atoms N3 and N4 of $H_2Imbzim^-$, while its benzimidazole nitrogen atoms N1 and N5 provide the sixth coordination site to the two metal centers. The equatorial planes of the two distorted octahedra are constituted by the atoms N1, N3, N4, N6 in **1**, N1, N3, N11, N13 and N4, N5, N8, N10 in **2**. The two pyridyl nitrogen atoms of each bpy ligand are coordinated alternatively in axial and equatorial modes.

In all three compounds, three types of metal−nitrogen distances are observed. The longest M−N distances involve the benzimidazole nitrogen atoms, with their values being 2.091(5) Å for **1**, 2.084(7) Å for **2**, and 2.077(5) Å for the diruthenium(II) compound. The next longest M−N distance pertaining to the imidazolate nitrogen atoms, whose average value is 2.045(4) Å, lies almost in the same range [2.035(7)−2.095(7) Å] of the M−N distances of the bpy ligands. The deviations of the metal centers from the idealized octahedral geometry can be gauged by considering the ranges of the trans angles, which lie between 167.0(2) and 176.5(3)°. In all of the three structures, it is seen that the two NH groups adopt a cis arrangement, and this pair of externally directed N−H protons of $H_2Imbzim^-$ could be used for formation of the adduct with the anions via a hydrogen-bonding interaction.

(32) *SAINT*, version 6.02; Bruker AXS Inc.: Madison, WI, 2002. *SADABS*, version 2.03; Bruker AXS Inc.: Madison, WI, 2002.
(33) Sheldrick, G. M. *SHELXL-97, Program for the Refinement of crystal Structures*; University of Göttingen: Göttingen, Germany, 1997.
(34) *SHELXTL*, version 6.10; Bruker AXS Inc.: Madison, WI, 2002.
(35) *PLATON*: Spek, A. L. *J. Appl. Crystallogr.* **2003**, *36*, 7.

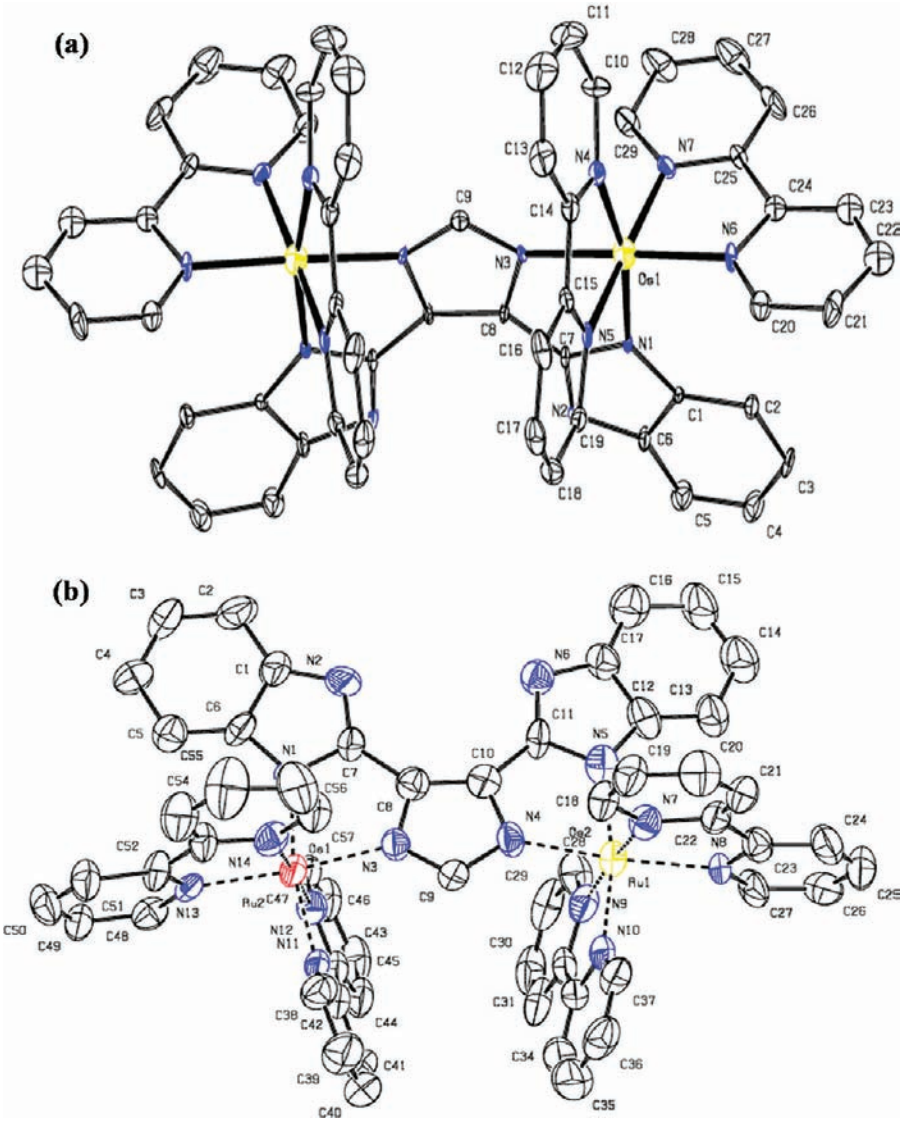

Figure 1. ORTEP representations of (a) $\mathbf{1}^{3+}$ and (b) $\mathbf{2}^{3+}$ showing 50% probability ellipsoid plots. Hydrogen atoms are omitted for clarity.

Two other important structural features, viz., the occurrence of aromatic $\pi-\pi$ and CH$-\pi$ interactions, deserve consideration. As may be noted in the capped-stick representation of both $\mathbf{1}^{3+}$ and $\mathbf{2}^{3+}$ (Figure S2, Supporting Information), the pyridine rings coordinated to Os^{II} by N4 and N5 are in face-to-face alignment with the pyridine rings that are coordinated to another Os^{II} by identical N4 and N5, while in compound **2**, the pyridine rings coordinated to Os^{II} by N11 and N12 are in face-to-face alignment with the pyridine rings that are coordinated to Ru^{II} by N10 and N9, respectively. The centroid$-$centroid distances between these two rings are 4.487 and 4.016 Å for **1** and 4.793 and 4.335 Å for **2**, respectively, while the respective dihedral angles between the ring planes are 41.9 and 35.6° for **1** and 43.8 and 44.8° for **2**. Clearly, the two heteroaromatic rings (4, 5/4, 5 in **1** and 11, 12/10, 9 in **2**) are involved in $\pi-\pi$ interaction. The same type of interaction also occurs in the previously reported analogous diruthenium(II) compound, which has the following values for centroid$-$centroid distances and dihedral angles: 4.465 and 4.028 Å and 42.3 and 35.7°[19a] (Figure S2, Supporting Information). It may be mentioned that perfect or near-perfect face-to-face alignment of the ring planes occurs rarely.[36,37] More usual are the cases of slipped-type $\pi-\pi$ interaction, where the ring planes are displaced in a parallel fashion.[36−38]

The occurrence of intramolecular CH$-\pi$ interactions in $\mathbf{1}^{3+}$, $\mathbf{2}^{3+}$, and the related diruthenium $[Ru^{II}Ru^{II}]^{3+}$ compound is also shown in Figure S2 (Supporting Information). In $\mathbf{1}^{3+}$, two hydrogen atoms H2 of the two phenyl rings are in close proximity to the centers of the pyridyl rings with the nitrogen atom N6, and in $\mathbf{2}^{3+}$, two hydrogen atoms H5 and H13 of the two phenyl rings are in close proximity to the centers of the pyridyl rings with the nitrogen atoms N13 and N8. The distances of both H2 of **1** and H5 and H13 of **2** from the centroids of the corresponding pyridyl rings are 2.727 Å in **1** and 2.833 and 2.804 Å in **2**, while the angle C2$-$H2$\cdots\pi$ (centroid of the N6$-$C20$\cdots$C24 ring) is 160.9° in **1** and C5$-$H5$\cdots\pi$ (centroid of the N13$-$C48$\cdots$C52 ring) and C13$-$H13$\cdots\pi$

(36) Janiak, C. *J. Chem. Soc., Dalton Trans.* **2000**, 3885.
(37) Wilson, S. R.; Moore, J. S. *Chem.—Eur. J.* **1997**, *3*, 765.
(38) Hunter, C. A.; Sanders, J. K. M. *J. Am. Chem. Soc.* **1990**, *112*, 5525.

Table 2. Selected Bond Distances (Å) and Angles (deg) for **1** and **2**

1		**2**			
Os−N4	2.041(5)	Os−N12	2.035(7)	Ru−N4	2.036(8)
Os−N5	2.045(5)	Os−N13	2.045(7)	Ru−N7	2.038(8)
Os−N3	2.047(4)	Os−N11	2.048(7)	Ru−N10	2.050(8)
Os−N7	2.052(5)	Os−N14	2.057(8)	Ru−N9	2.068(8)
Os−N6	2.058(5)	Os−N3	2.057(7)	Ru−N5	2.082(9)
Os−N1	2.091(5)	Os−N1	2.084(7)	Ru−N8	2.095(7)
Os---Os	6.136	Ru---Os	6.205		
N4−Os−N5	78.3(2)	N12−Os−N13	98.6(3)	N4−Ru−N7	96.2(3)
N4−Os−N3	91.7(2)	N12−Os−N11	79.1(3)	N4−Ru−N10	92.8(3)
N5−Os−N3	86.00(18)	N13−Os−N11	93.0(3)	N7−Ru−N10	96.7(3)
N4−Os−N7	98.4(2)	N12−Os−N14	176.5(3)	N4−Ru−N9	86.5(3)
N5−Os−N7	175.4(2)	N13−Os−N14	79.4(3)	N7−Ru−N9	174.7(3)
N3−Os−N7	97.46(19)	N11−Os−N14	98.1(3)	N10−Ru−N9	78.6(4)
N4−Os−N6	94.1(2)	N12−Os−N3	85.9(3)	N4−Ru−N5	76.4(3)
N5−Os−N6	97.6(2)	N13−Os−N3	174.1(3)	N7−Ru−N5	89.4(3)
N3−Os−N6	173.67(19)	N11−Os−N3	91.6(3)	N10−Ru−N5	168.1(3)
N7−Os−N6	79.2(2)	N14−Os−N3	96.4(3)	N9−Ru−N5	95.7(3)
N4−Os−N1	167.0(2)	N12−Os−N1	94.9(3)	N4−Ru−N8	174.0(3)
N5−Os−N1	95.2(2)	N13−Os−N1	99.0(3)	N7−Ru−N8	79.6(3)
N3−Os−N1	76.50(18)	N11−Os−N1	167.4(3)	N10−Ru−N8	92.0(3)
N7−Os−N1	88.7(2)	N14−Os−N1	88.2(3)	N9−Ru−N8	98.0(3)
N6−Os−N1	97.93(18)	N3−Os−N1	76.7(3)	N5−Ru−N8	99.1(3)

(centroid of the N8−C23···C27 ring) are 157.2° and 160.7°, respectively. The implication of these point-to-face or edge-on CH−π interactions[39,40] on the ^{1}H NMR spectra of the compounds will be seen later. Further, the hydrogen atoms H29 of the pyridyl rings C25···C29−N7 in **1** and H57 and H18 of the pyridyl rings C53···C57−N14 and C18···C22−N7 in **2** are close to the center of the imidazolate ring π cloud, and corresponding distances and angles are 3.302 Å and 134.9° in **1** and 3.251 and 3.228 Å and 136.6 and 134.5° in **2**, respectively. Similar interactions that occur with the $Ru^{II}Ru^{II}$ compound and the metrical parameters involved therein can be seen in Figure S2 (Supporting Information).

^{1}H NMR Spectra. The ^{1}H NMR spectra of the complexes have been recorded in $(CD_3)_2SO$, and their chemical shift values are given in the Experimental Section. The spectral assignments made for the observed chemical shifts of the bridging $H_2Imbzim^-$ ligand as well as the bipyridine protons in the complexes according to the numbering scheme (shown in Scheme 1), aided by $\{^1H-^1H\}$ COSY NMR spectra have been made in the same way as reported earlier.[15,19]

For both of the bimetallic complexes, all of the resonances, barring two, occur in the range 6.85−8.85 ppm. Of the two disparate signals, the one that is most shielded among all appears as a doublet between 5.04 and 5.64 ppm and is clearly due to H14 (Scheme 1 for proton labeling) because this proton experiences maximum diamagnetic shielding by the anisotropic ring current of the adjacent bipyridine rings (Figure S2, Supporting Information). As was already noted in Figure S2 in the Supporting Information, the phenyl ring protons H2 in **1** and H5 and H13 in **2** of the bridging ligand are very close to the centroids of the pyridyl rings having the nitrogen atoms N6 in **1** and N13 and N8 in **2**, respectively. In solution, the two slightly different CH−π distances are averaged and observed as a

Scheme 1

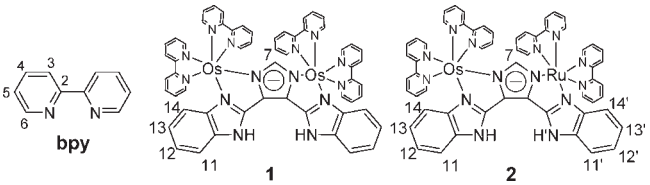

single resonance in the ^{1}H NMR spectrum. It should be noted that the two hydrogen atoms H2 of **1** in Figure 1a are referred to as H14 in Scheme 1, while H5 and H13 of **2** in Figure 1b are referred to as H14/H14′ in Scheme 1. Aside from H2, H5, and H13, other phenyl protons are not sterically oriented for CH−π interaction to experience the ring current effect. The most downfield-shifted resonances in $\mathbf{1}^{3+}$ (13.7 ppm) and $\mathbf{2}^{3+}$ (13.65 and 13.58 ppm) are due to the benzimidazole NH, which are hydrogen-bonded to $(CD_3)_2SO$. The ^{1}H NMR spectrum of the heterobimetallic complex $[(bpy)_2Ru^{II}(H_2Imbzim)Os^{II}(bpy)_2]^{3+}$ ($\mathbf{2}^{3+}$) is complicated compared to those of their homodinuclear analogues $Os^{II}Os^{II}$ and $Ru^{II}Ru^{II}$ because of the presence of many signals and extensive overlapping. The two benzimidazole units of $H_2Imbzim^-$ in $\mathbf{2}^{3+}$ are no longer magnetically equivalent, and, accordingly, two sets of resonances due to the NH, H11−H14, and H11′−H14′ protons can be expected to be observed.

Absorption Spectral Studies. The UV−vis spectral data of both complexes **1** and **2** and the previously reported diruthenium(II) complex in dichloromethane are catalogued in Table 3. All of the compounds, in general, exhibit quite a large number of peaks and shoulders. Three main regions can be distinguished: from 200 to 400 nm, the spectra are dominated by very intense absorption bands (ε = 31 000−159 400 M^{-1} cm^{-1}), while between 400 and 550 nm, there are moderately intense bands (ε = 21 550−30 740 M^{-1} cm^{-1}). Complexes **1** and **2** show additional broad and weaker spectral features (ε = 2500−5120 M^{-1} cm^{-1}) in the longer-wavelength region (600−800 nm). On the basis of the extensive investigations performed on $[Ru(bpy)_3]^{2+}$ and $[Os(bpy)_3]^{2+}$ and related complexes,[14,15]

(39) Nishino, M.; Hirota, M.; Umezawa, Y. *The CH/π Interaction: Evidence, Nature and Consequences*; Wiley-VCH: New York, 1998.

(40) Desiraju, G. R.; Steiner, T. *The Weak Hydrogen Bond in Structural Chemistry and Biology*; Oxford Science Publishers, Oxford, U.K., 1999.

Table 3. Absorption Spectral Data for the Complexes in Dichloromethane

	λ_{max}, nm (ε, M^{-1} cm^{-1})		
compound	without added anion	with 6 equiv of added anion	$\Delta\lambda$, nm
$Ru^{II}Ru^{II}$[a]	489 (28 970)	506 (22 550)	17 (489 → 506)
	450 (30 740)	464 (sh) (18 990)	14 (450 → 464)
	380 (sh) (34 870)	364 (54 000)	
	355 (53 800)	290 (br) (14 100)	
	335 (44 960)		
	292 (159 400)		
	242 (97 400)		
$Os^{II}Os^{II}$	705 (br) (4370)	800 (br) (5530)	95 (705 → 800)
	638 (br) (5120)	725 (br) (5540)	87 (638 → 725)
	505 (21 550)	555 (20 000)	50 (505 → 555)
	462 (22 200)	530 (sh) (19 330)	68 (462 → 530)
	417 (24 700)	360 (br) (50 900)	
	363 (35 900)	295 (111 700)	
	342 (31 000)	245 (95 900)	
	292 (98 200)		
	245 (60 700)		
$Ru^{II}Os^{II}$	705 (br) (2500)	760 (br) (3330)	55 (705 → 760)
	637 (br) (2900)	530 (21 650)	45 (485 → 530)
	485 (27 600)	360 (53 930)	79 (451 → 530)
	451 (29 400)	292 (br) (113 170)	
	392 (32 000)	242 (102 200)	
	358 (51 600)		
	340 (44 700)		
	292 (112 600)		
	245 (82 100)		

[a] Reference 19a.

it can be deduced that the high-intensity absorption bands in the 200−400 nm spectral region are due to the $\pi-\pi^*$ transition of bipyridine and spin-allowed ligand-centered transitions of the bridging ligand and the absorption bands in the 400−550 nm region are due to spin-allowed metal-to-ligand {Ru/Os (dπ) → bpy and/or $H_2Imbzim^-$ (π^*)} charge-transfer (MLCT) transitions. The weak and broad spectral bands that appeared in the range between 600 and 800 nm for both **1** and **2** are due to a spin-forbidden MLCT transition that directly populates the triplet MLCT state of bpy and $H_2Imbzim^-$. In Figure 2, the UV−vis spectra of equimolar solutions of $Ru^{II}Ru^{II}$, $Os^{II}Os^{II}$, and $Ru^{II}Os^{II}$ in dichloromethane at room temperature are displayed.

Luminescence Spectra. The emission spectral behavior of the complexes has been studied in dichloromethane or acetonitrile solutions at room temperature and at 77 K in ethanol−methanol (4:1) glass. Table 4 summarizes the emission maxima, quantum yields, and lifetimes of three bimetallic complexes. Figure 3 compares the photoluminescence spectra of equimolar solutions of $Ru^{II}Os^{II}$ and of its homometallic parents $Ru^{II}Ru^{II}$ and $Os^{II}Os^{II}$ (λ_{exc} = 505 nm) at both room temperature and 77 K. It is well-known that diimine complexes of Ru^{II} typically absorb in the visible region via Ru (dπ) to diimine (π^*) MLCT transitions. Very rapid intersystem crossing follows to populate the ^{3}MLCT state. This state decays to the ground state via a combination of radiative and nonradiative processes with lifetimes that vary between a few nanoseconds to a few microseconds. On the other hand, osmium(II) complexes have absorption maxima for the spin-allowed MLCT absorption at wavelengths similar to those of ruthenium(II) but also exhibit the spin-forbidden ^{1}GS to ^{3}MLCT state absorption at longer wavelengths. The osmium(II) complexes generally exhibit emission from the ^{3}MLCT state at longer wavelengths and with much lower efficiencies than the corresponding ruthenium(II)

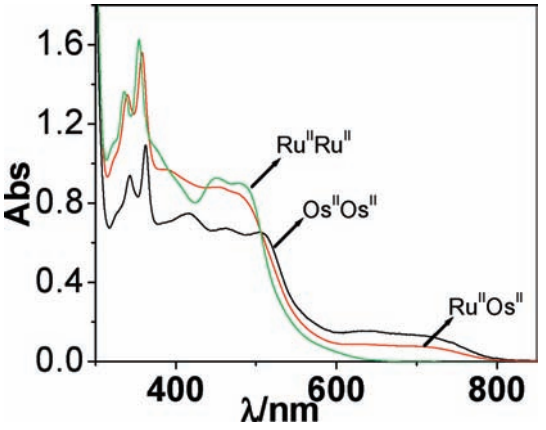

Figure 2. Absorption spectra of equimolar solutions of $[Ru^{II}Ru^{II}]^{3+}$, $[Os^{II}Os^{II}]^{3+}$ (**1**), and $[Ru^{II}Os^{II}]^{3+}$ (**2**) in dichloromethane at room temperature.

complexes. Excited-state lifetimes of the osmium(II) complexes are generally between 50 and 500 ns in solution.[14,15] It has also been reported in the literature that relatively small changes in the coordination environment can lead to large differences in the photophysical behavior of the complexes. In complex **2**, two overlapping emission bands are seen in the spectral range 600−900 nm, the deconvolution (Figure 3, inset) of which gives rise to two peaks at 653 and 780 nm in dichloromethane at room temperature and at 640 and 710 nm in ethanol−methanol glass at 77 K. By comparison with the emission spectra of the homodinuclear complexes, the bands at 653 and 640 nm seem to be due to emission from the Ru^{II}-centered moiety and the bands at 780 and 710 nm due to the Os^{II}-centered moiety. The close similarity of the band positions observed between excitation and absorption spectra indicates that the observed emission bands are indeed due to the complexes

Table 4. Luminescence Spectral Data for the Complexes

	298 K[a]								77 K[b]			
	Ru-based				Os-based				Ru-based		Os-based	
compound	λ_{max}, nm	Φ	τ, ns	I	λ_{max}, nm	Φ	τ, ns	I	λ_{max}, nm	Φ	λ_{max}, nm	Φ
$Ru^{II}Ru^{II}$[c]	660	8.56×10^{-2}	190	983					645	1.9×10^{-1}		
$Os^{II}Os^{II}$					780	1.1×10^{-3}	50	15			710	1.2×10^{-2}
$Ru^{II}Os^{II}$	653	1.51×10^{-2}	15	152	780	8.5×10^{-3}	48	38	640	1.6×10^{-1}	710	1.0×10^{-1}

[a] In a dichloromethane solution. [b] In 4:1 ethanol−methanol glass. [c] Reference 19a.

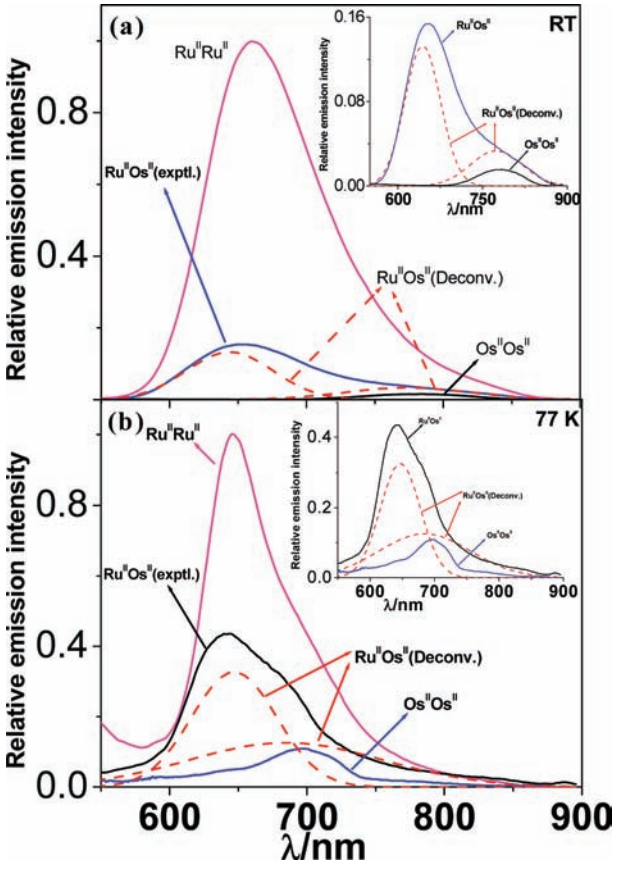

Figure 3. Luminescence spectra of equimolar solutions of $[Ru^{II}Ru^{II}]^{3+}$, $[Os^{II}Os^{II}]^{3+}$ (**1**), and $[Ru^{II}Os^{II}]^{3+}$ (**2**) at room temperature in dichloromethane (a) and at 77 K in 4:1 ethanol−methanol glass (b). The inset shows both the observed and deconvoluted spectra of **2**.

(Figure S3, Supporting Information). On going from a fluid solution to frozen glass, the emission maxima get blue-shifted with a significant increase of the intensities and the quantum yields, which are the characteristics of typical MLCT emitters.[14,15] It is to be noted that the strong luminescence band at 465 nm due to free H_3Imbzim in fluid solution at room temperature is completely quenched in the metal complexes by energy transfer to the metal-based units, which exhibit their characteristic MLCT phosphorescence.

Redox Activities. The electrochemical behavior of the complexes has been studied in acetonitrile by CV and SWV methods, and the relevant results are given in Table 5. In all of the cases, the metal-centered oxidations take place reversibly. Complex **1** displays two successive one-electron oxidation waves, and the $E_{1/2}$ values for $Os^{II}Os^{II}$/$Os^{II}Os^{III}$ and $Os^{II}Os^{III}$/$Os^{III}Os^{III}$ couples are 0.42 and 0.55 V, respectively. Taking into consideration the $E_{1/2}$ values reported for the diruthenium(II) complex, the first couple observed for **2** at 0.53 V can be attributed to the $Os^{II}Ru^{II}$/$Os^{III}Ru^{II}$ couple, while the second couple observed at 1.07 V is due to the $Os^{III}Ru^{II}$/$Os^{III}Ru^{III}$ process. The cyclic voltammograms recorded up to −2.2 V exhibit two quasi-reversible reductions (see Table 5). As shown in Figure S4 (Supporting Information), the current heights observed in both CV and SWV are almost double for a reduction wave compared to that of an oxidation wave, indicating that the simultaneous transfer of two electrons occurs in the reduction processes.

The separation between the two oxidation potentials ($\Delta E_{1/2} = |E_{1/2}(\mathbf{1}) - E_{1/2}(\mathbf{2})|$) in the homodinuclear complexes (Table 5) provides information about the extent of electronic interactions involved between the two metal centers. The $\Delta E_{1/2}$ value of the diosmium complex (0.13 V) is smaller than that of the previously reported diruthenium analogue (0.19 V). For covalently linked bimetallic systems, the electronic coupling between the two metal centers is mediated by the bridging ligand whose length, rigidity, charge, and conjugation regulate the extent of electron delocalization.[14] Depending upon the type of bridging ligand, which may have either low-lying π^*-acceptor orbital(s) or electron-rich high-lying π^*-donor orbitals, metal−metal interaction occurs through superexchange-assisted electronic coupling via an electron-transfer or a hole-transfer mechanism, respectively.[14,41] Neutral ligands with extensive delocalization act as π acceptors, while anionic ligands behave as π donors. In the case of the electron-transfer mechanism, metal−metal interaction occurs via efficient mixing of the higher dπ orbitals of the metal centers with the π^* orbitals (lowest unoccupied molecular orbital) of the bridging ligand. On the other hand, for the hole-transfer mechanism, coupling occurs between the highest occupied molecular orbital of the bridge [occupied π-bridge orbital(s)] and the metal dπ orbitals.[42] Generally, when the bridging ligand is of the π-acceptor type, the difference between the first and second oxidation potentials is larger for Os^{II} dimers compared to Ru^{II} dimers.[14c,43] In the present case, the bridging H_3Imbzim ligand acts as a π-donor type because the central

(41) (a) Richardson, D. E.; Taube, H. *J. Am. Chem. Soc.* **1983**, *105*, 40. (b) Newton, M. D. *Chem. Rev.* **1991**, *91*, 767. (c) Jordan, K. D.; Paddon-Row, M. N. *Chem. Rev.* **1992**, *92*, 395. (d) Todd, M. D.; Nitzan, A.; Ratner, M. A. *J. Phys. Chem.* **1993**, *97*, 29.

(42) (a) Barigelletti, F.; De Cola, L.; Balzani, V.; Hage, R.; Haasnoot, J. G.; Reedijk, J.; Vos, J. G. *Inorg. Chem.* **1989**, *28*, 4344. (b) Barigelletti, F.; De Cola, L.; Balzani, V.; Hage, R.; Haasnoot, J. G.; Reedijk, J.; Vos, J. G. *Inorg. Chem.* **1991**, *30*, 641. (c) Haga, M. *Inorg. Chim. Acta* **1983**, *75*, 29. (d) Haga, M.; Bond, A. M. *Inorg. Chem.* **1991**, *30*, 475.

(43) (a) Denti, G.; Campagna, S.; Sabatino, L.; Ciano, M.; Balzani, V. *Inorg. Chem.* **1990**, *29*, 4750. (b) Denti, G.; Serroni, S.; Sabatino, L.; Ricevuto, V.; Ciano, M.; Campagna, S. *Gazz. Chem. Ital.* **1991**, *12*, 37.

Table 5. Electrochemical Data for the Complexes in Acetonitrile

	oxidation potential (V)								reduction potential (V)			excited state potential (eV)[b]	
	without added anion				with 6 equiv of added anion				without added anion			without added anion	
compound	$M^{II}M^{II}/M^{II}M^{III}$ $E_{1/2}(1)$	$M^{II}M^{III}/M^{III}M^{III}$ $E_{1/2}(2)$	$\Delta E_{1/2} = [E_{1/2}(2) - E_{1/2}(1)]$	K_c	$M^{II}M^{II}/M^{II}M^{III}$ $E_{1/2}(1)$	$M^{II}M^{III}/M^{III}M^{III}$ $E_{1/2}(2)$	$\Delta E_{1/2} = [E_{1/2}(2) - E_{1/2}(1)]$	K_c			E_{00} (eV)	$E^*_{ox(n)}$ $(n = 1, 2)$	$E^*_{red(n)}$ $(n = 1, 2)$
$Ru^{II}Ru^{II}$[a]	0.92	1.11	0.19	1.6×10^3	0.66	1.11	0.45	1.3×10^7	−1.45, −1.77	2.12		−1.20, −1.01	0.67, 0.35
$Os^{II}Os^{II}$	0.42	0.55	0.13	1.6×10^2	0.15				−1.71, −2.02	1.74		−1.32, −1.19	0.03, −0.28
$Ru^{II}Os^{II}$	0.53	1.07	0.54		0.32	0.64	0.32		−1.45, −1.73	2.16, 1.74		−1.09, −1.21	0.71, 0.29

[a] Reference 19a. [b] Obtained from eqs 3 and 4.

imidazole NH proton gets deprotonated and produces monoanionic $H_2Imbzim^-$ during formation of the binuclear complex.

Table 5 summarizes the ground- and excited-state redox potentials of the complexes. The excited-state redox potentials can be calculated by using eqs 3 and 4.[14]

$$E*_{ox(n)}([M^{II}M^{III}]/[M^{II}M^{II}]) = E_{1/2(n)}([M^{II}M^{III}]/[M^{II}M^{II}]) - E_{00} \quad n = 1, 2 \quad (3)$$

$$E*_{red(n)}([M^{II}M^{II}(lig)]/[M^{II}M^{II}(lig^{\bullet\bullet - -})]) = E_{1/2(n)}([M^{II}M^{II}(lig)]/[M^{II}M^{II}(lig^{\bullet\bullet - -})]) + E_{00} \quad n = 1, 2 \quad (4)$$

In these relations, E_{00} are the zero−zero excitation energies of the complexes, which can be obtained at the intersection of the absorption and emission bands.

Intercomponent Energy Transfer in 2. As was already mentioned, a comparison of the deconvoluted luminescence spectrum of the $Os^{II}Ru^{II}$ complex (**2**) with corresponding $Os^{II}Os^{II}$ (**1**) and $Ru^{II}Ru^{II}$ complexes indicate that the peak observed in **2** at 780 nm (298 K) or at 710 nm (77 K) is due to the Os^{II} center, while the peak at 653 nm (298 K) or at 640 nm (77 K) is due to the Ru^{II} center. It is important to note that the quantum yield and the lifetime of the Ru^{II}-centered emission in **2** are considerably less compared to those of the diruthenium(II) complex. This indicates that the Os^{II}-centered moiety probably induces a quenching effect on the Ru^{II}-centered component. Similar quenching of Ru^{II} luminescence in heterobimetallic $Os^{II}Ru^{II}$ complexes has been reported in the literature.[14,18,44] We have estimated the extent of Ru^{II} luminescence quenching by adopting these reported procedures, which involve measurement of the luminescent intensities of three isomolar solutions of $Ru^{II}Ru^{II}$, $Os^{II}Ru^{II}$, and $Os^{II}Os^{II}$ complexes by excitation at the wavelength where the isosbestic point is observed in their absorption spectra, while keeping identical experimental conditions in all cases. The result obtained shows that 85% of the luminescence intensity of the Ru^{II}-based component is quenched by the Os^{II}-based component. Further, a comparison of the intensities of the Os^{II}-based luminescence (at 780 nm) in the $Os^{II}Ru^{II}$ complex with that of the $Os^{II}Os^{II}$ species and correcting for the tail of the residual Ru^{II}-based luminescence reveals that they coincide within experimental error (Figure 3). Because Os^{II} is easier to oxidize than Ru^{II} in polypyridine complexes, the MLCT levels of Ru^{II} are placed at higher energies than their Os^{II} counterparts.[14,44] In the present case, the excited-state energy of the Ru^{II}-based component is 2.16 eV, while that of the Os^{II}-based component is 1.74 eV (Figure S5, Supporting Information). Therefore, the free-energy change (neglecting entropy changes) for energy transfer from an

(44) (a) Belser, P.; von Zelewsky, A.; Frank, M.; Seel, C.; Vögtle, F.; De Cola, L.; Barigelletti, F.; Balzani, V. *J. Am. Chem. Soc.* **1993**, *115*, 4076. (b) De Cola, L.; Balzani, V.; Barigelletti, F.; Flamigni, L.; Belser, P.; von Zelewsky, A.; Frank, M.; Vögtle, F. *Inorg. Chem.* **1993**, *32*, 5228. (c) Schlicke, B.; Belser, P.; De Cola, L.; Sabbioni, E.; Balzani, V. *J. Am. Chem. Soc.* **1999**, *121*, 4207. (d) Barigelletti, F.; Flamigni, L.; Balzani, V.; Collin, J.-P.; Sauvage, J.-P.; Sour, A.; Constable, E. C.; Cargill Thompson, A. M. W. *J. Am. Chem. Soc.* **1994**, *116*, 7692.

excited-state Ru^{II}-based component to a ground-state Os^{II}-based component is approximately −0.42 eV. This thermodynamically favored process accounts for the observed quenching.

It should be noted in this context that quenching, in principle, can take place by an electron-transfer process also. However, to be feasible, the process has to be thermodynamically favorable. For example, the photoinduced oxidative quenching in **2**

$$^{*}Ru^{II}Os^{II} \rightarrow Ru^{III}Os^{I} \quad (5)$$

$$\Delta G^{\circ} = E^{\circ}([Ru^{III}Os^{II}]^{4+}/[Ru^{II}Os^{II}]^{3+}) - E^{\circ}([Ru^{II}Os^{II}(lig)]^{3+}/[Ru^{II}Os^{II}(lig^{\bullet -})]^{+}) - E_{00} \quad (6)$$

is highly unfavorable because the free-energy change according to eq 6 is too high, + 0.36 eV. On the other hand, the reductive quenching process

$$^{*}Ru^{II}Os^{II} \rightarrow Ru^{I}Os^{III} \quad (7)$$

$$\Delta G^{\circ} = E^{\circ}([Ru^{II}Os^{III}]^{4+}/[Ru^{II}Os^{II}]^{3+}) - E^{\circ}([Ru^{II}Os^{II}(lig)]^{3+}/[Ru^{II}Os^{II}(lig^{\bullet -})]^{+}) - E_{00} \quad (8)$$

although slightly exoergonic (−0.18 eV), is still unfavorable probably because of the large reorganization energy in a polar solvent. By contrast, quenching via energy transfer

$$^{*}Ru^{II}Os^{II} \rightarrow Ru^{II*}Os^{II} \quad (9)$$

is strongly exoergonic (−0.42 eV) and hence highly favorable.

In Figure 4, the luminescence decay profiles of Ru^{II}-Ru^{II}, $Os^{II}Os^{II}$, and $Os^{II}Ru^{II}$ in dichloromethane at room temperature are shown. It may be noted that, in the cases of $Ru^{II}Ru^{II}$, $Os^{II}Os^{II}$, and Ru^{II}-centered $Os^{II}Ru^{II}$, all exhibit monophasic decay with lifetimes of 190, 50, and 187 ns, respectively. Interestingly, the Os^{II}-centered decay of the $Os^{II}Ru^{II}$ complex undergoes biexponential decay with lifetimes of 15 and 48 ns. Close agreement between the lifetimes of 50 ns (in $Os^{II}Os^{II}$) and 48 ns (Os^{II} in $Os^{II}Ru^{II}$) is gratifying to note.

The rate constant, k_{en}, for energy transfer can be calculated by using eq 10

$$k_{en} = \frac{1}{\tau} - \frac{1}{\tau^{0}} \quad (10)$$

where τ^{0} is the emission lifetime of the $Ru^{II}Ru^{II}$ complex (190 ns) and τ is the luminescence lifetime (15 ns) of the Ru^{II}-centered $Os^{II}Ru^{II}$ complex. Thus, the value of k_{en} at room temperature is 6.1×10^{7} s^{-1}. The reason for such fast energy transfer is likely due to overlap between donor emission (λ_{max} = 653 nm) and acceptor absorption (lying between 635 and 750 nm).

In the literature, intramolecular energy-transfer rates of several types of $Ru^{II}Os^{II}$ complexes have been reported.

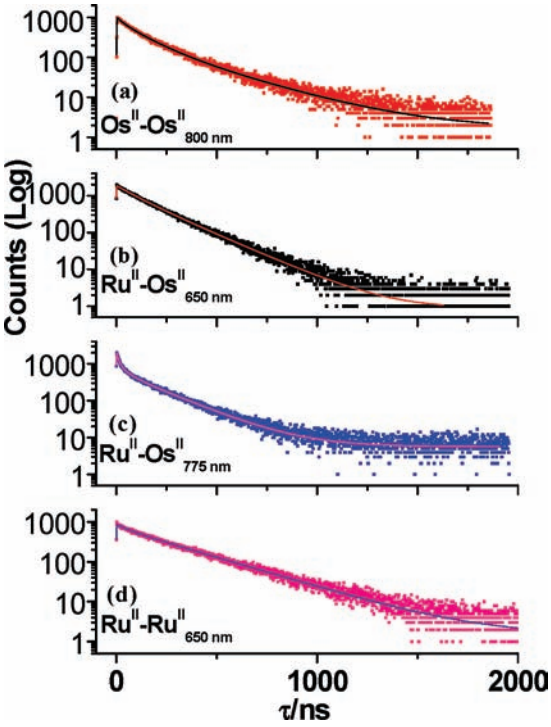

Figure 4. Time-resolved photoluminescence decays of equimolar solutions of $[Ru^{II}Ru^{II}]^{3+}$, $[Os^{II}Os^{II}]^{3+}$ (**1**), and $[Ru^{II}Os^{II}]^{3+}$ (**2**) at room temperature in dichloromethane obtained with 440 nm excitation.

Energy-transfer processes occur in two ways, viz., the Dexter-type[45] through bond electron exchange and the Förster-type[46] through space Coulombic interaction. However, in most cases, it is not easy to ascertain which particular mechanism plays the dominant role. Electron exchange becomes important where the spacer is either highly conjugated or relatively short, while the Coulombic mechanism becomes important when either the spacer is saturated or the transition dipoles are well-separated.[47]

$Ru^{II}Os^{II}$ complexes containing alkyne-type spacers have been found to exhibit efficient triplet energy transfer from Ru → Os on a picosecond time scale ($k_{en} > 10^{10}$ s^{-1}).[48] Similar very fast energy-transfer processes have been reported for the complexes in which the chelating units are separated by one or two phenyl rings.[44,49] In contrast, compounds in which the spacers contain a saturated moiety, such as bicyclo[2,2,2]octane, adamantine, etc., interposed between two phenyl rings, have been found to slow down the Ru → Os energy-transfer rate remarkably ($k_{en} \sim 10^{6}$ s^{-1}).[44b,47,50] In our case, where the bridging unit

(45) Dexter, D. L. *J. Chem. Phys.* **1953**, *21*, 836.
(46) Förster, T. H. *Discuss. Faraday Soc.* **1996**, *27*, 7.
(47) De Cola, L.; Belser, P. *Coord. Chem. Rev.* **1998**, *177*, 301.
(48) (a) Benniston, A. C.; Grosshenny, V.; Harriman, A.; Ziessel, R. *Angew. Chem., Int. Ed. Engl.* **1994**, *33*, 1884. (b) Harriman, A.; Ziessel, R. *J. Chem. Soc., Chem. Commun.* **1996**, 1707. (c) Grosshenny, V.; Harriman, A.; Ziessel, R. *Angew. Chem., Int. Ed. Engl.* **1995**, *34*, 1100.
(49) (a) Schmehl, R. H.; Auerbach, R. A.; Walcholtz, W. F. *J. Phys. Chem.* **1988**, *92*, 6202. (b) Baba, A. I.; Ensley, H. E.; Schmehl, R. H. *Inorg. Chem.* **1995**, *34*, 1198. (c) Barigelletti, F.; Flamigni, L.; Balzani, V.; Collin., J.-P.; Sauvage, J.-P.; Sour, A.; Constable, E. C.; Cargill Thompson, A. M. W. *J. Chem. Soc., Chem. Commun.* **1993**, 942. (d) Barigelletti, F.; Flamigni, L.; Balzani, V.; Collin., J.-P.; Sauvage, J.-P.; Sour, A.; Constable, E. C.; Cargill Thompson, A. M. W. *Coord. Chem. Rev.* **1994**, *132*, 209.
(50) (a) De Cola, L.; Balzani, V.; Barigelletti, F.; Flamigni, L.; Belser, P.; Bernhard, S. *Recl. Trav. Chim. Pays-Bas* **1995**, *114*, 534. (b) Balzani, V.; Barigelletti, F.; Belser, P.; Bernhard, S.; De Cola, L.; Flamigni, L. *J. Phys. Chem.* **1996**, *100*, 16786.

Figure 5. Color changes that occur when the acetonitrile solutions of the receptors **1** (a) and **2** (b) are treated with various anions as their TBA salts.

contains the $[H_2Imbzim]^-$ anion, the Ru → Os energy-transfer rate is moderately fast ($k_{en} = 6.1 \times 10^7\ s^{-1}$). A similar order of k_{en} has been reported for a triazolate anion-bridged $Ru^{II}Os^{II}$ complex.[51]

Anion-Sensing Studies. Color Changes of the Receptors in Solution upon Interaction with Anions. The anion-sensing ability of the receptors **1** and **2** has been studied on a qualitative basis by visual examination of the anion-induced color changes in acetonitrile solutions (2.0×10^{-5} M) before and after the addition of an anion. TBA salts of F^-, Cl^-, Br^-, I^-, HSO_4^-, and AcO^- ions have been used as substrates for the receptors. The photograph in Figure 5 shows the dramatic color changes of **1** and **2** in the presence of F^- and AcO^- ions only, while in contrast, the anions Cl^-, Br^-, I^-, and HSO_4^- induce almost no change in color. Evidently, there is a strong interaction between the receptors with the substrate anions F^- and AcO^- and a very weak or almost no interaction with the other anions.

^{1}H NMR Spectral Changes of the Receptors upon Interaction with Anions. Sensing of the anions by the metalloreceptors has been monitored by observing the ^{1}H NMR spectral changes that occur with the incremental addition of anions to their DMSO-d_6 solutions. Upon a gradual addition of the F^- ion to the solution of **2**, the chemical shifts of two N−H protons of $H_2Imbzim^-$ that initially appeared as a pair of singlets at 13.58 and 13.65 ppm get broadened, shifted to downfield, and finally vanished (see Figure S6, Supporting Information). Importantly, as shown in Figure 6, the signals of the H11, H12, H13, and H14 protons of **2** undergo a progressive upfield shift until 1 equiv of the F^- ion is added, beyond which no further change occurs. A similar behavior is also observed with the AcO^- ion. The ^{1}H NMR spectral change of **1** that occurs with the addition of an excess of the AcO^- ion is shown in Figure 7.

Absorption Spectral Changes of the Receptors upon Interaction with Anions. Sensing of the anions by the metalloreceptors has been monitored by observing the spectral changes that occur in acetonitrile solutions. As shown in Figure 8, the MLCT peaks at 708 and 507 nm

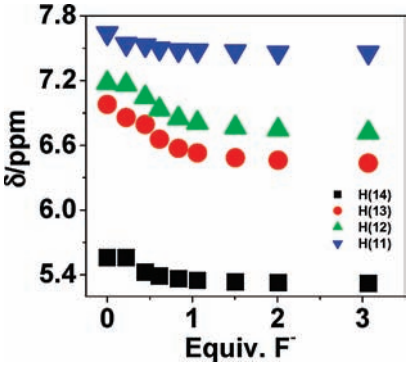

Figure 6. Change of the chemical shifts for the H_{11}, H_{12}, H_{13}, and H_{14} protons of $H_2Imbzim^-$ in $\mathbf{2}^{3+}$ as a function of the equivalents of F^- added.

for **1** and at 705 and 490 nm for **2** remain practically unchanged upon the addition of 8 equiv of Cl^-, Br^-, I^-, and HSO_4^- ions to 2.5×10^{-5} M solutions of **1** (Figure 8a) and **2** (Figure 8b). On the other hand, following the addition of 8 equiv of F^- and AcO^-, the MLCT bands get red-shifted to 790 and 545 nm for **1** and to 760 and 530 nm for **2**, respectively, indicating that strong interactions occur between the receptors and anions. These observations are in consonance with the visual changes already noted in Figure 5. The red shift of the MLCT bands can be attributed to the second-sphere donor−acceptor interactions between metal-coordinated $H_2Imbzim^-$ and the anions.[52] Such interactions (hydrogen bonding or proton transfer, vide infra) increase the electron density at the metal center, leading to lowering of the MLCT band energies.

In order to gain quantitative insight into sensor−anion interaction, spectrophotometric titrations have been carried out with F^- and AcO^- ions. The spectral changes that occur for **1** as a function of F^- are shown in Figure 9a−c. As may be noted, with an increase of F^- up to 1 equiv, the MLCT bands in the successive absorption curves undergo red shifts, during which they pass through four isosbestic points at 656, 605, 365, and 345 nm. Upon further addition, these bands (740, 520, and 462 nm) undergo a continual red shift until the absorption maxima at 790 and 545 nm are reached at ca. 8 equiv of F^-. During this process, the absorption curves pass through a new set of isosbestic points at 740, 644, 545, and 395 nm.

Similar trends of spectral changes have been observed for **2** as a function of F^- (shown in Figure 9d−f). As the F^- ion is added to a solution of **2**, the MLCT absorption maxima at 705 and 490 nm get shifted to longer wavelengths, viz., 755 and 495 nm, respectively, with the concurrent development of four isosbestic points at 676, 620, 498, and 413 nm upon the addition of 1 equiv of F^-. Upon continual addition beyond 1 equiv, these bands undergo further red shift until the absorption maxima at 760 and 530 nm are reached at ca. 8 equiv of F^-. During this process, the absorption curves pass through a new set of isosbestic points at 705, 515, and 395 nm. The spectral behavior observed with AcO^- as the guest anions is almost identical with that of F^- for both **1** and **2** (Figure S7, Supporting Information).

By using eq 1, the equilibrium constant K for receptor−anion interaction has been evaluated, and the values are

(51) Weldon, F.; Hammarström, L.; Mukhtar, E.; Hage, R.; Gunneweg, E.; Haasnoot, J. G.; Reedijk, J.; Browne, W. R.; Guckian, A. L.; Vos, J. G. *Inorg. Chem.* **2004**, *43*, 4471.

(52) Balzani, V.; Sabbatini, N.; Scandola, F. *Chem. Rev.* **1986**, *86*, 319.

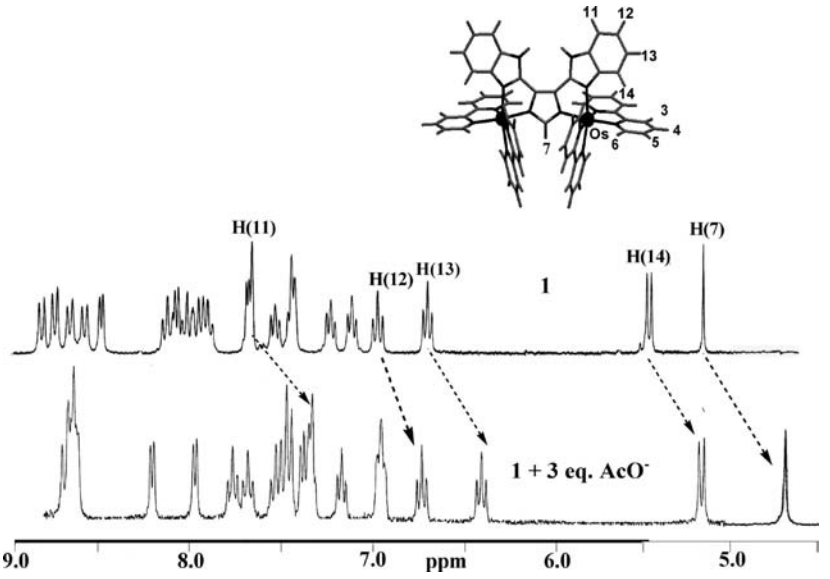

Figure 7. ^{1}H NMR spectra of $\mathbf{1}^{3+}$ in the presence and absence of the AcO^- ion in DMSO-d_6.

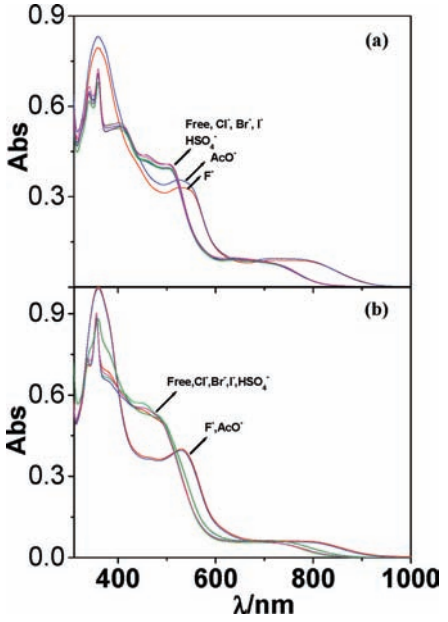

Figure 8. Changes in the UV−vis spectra of receptors **1** (a) and **2** (b) in acetonitrile upon the addition of different anions as TBA salts.

given in Table 6. It may be noted that the values of K for the receptors with F^- and AcO^- are grossly of 6 orders of magnitude. Comparable values of the equilibrium constant of a related diruthenium(II) complex with anionic guests such as F^- and AcO^- have been reported previously.[19a]

It was reported previously that suitably substituted hydrogen-bond-donor receptor functionality undergoes deprotonation in the presence of excess anions, leading to classical Brønsted acid−base chemistry.[53] To examine such a possibility, spectrophotometric titrations of the metalloreceptors (**1** and **2**) have also been carried out with a solution of TBAOH (Figure S8, Supporting Information). The spectral patterns for the complexes have close resemblance to the spectra of these receptors in the presence of F^- and AcO^- ions.

Emission Spectral Changes of the Receptors upon Interaction with Anions. Parts a and b of Figure 10 show that the emission intensity of the band at 780 nm for **1** and at 670 nm for **2** undergoes nominal change with the addition of Cl^-, Br^-, I^-, and HSO_4^- ions. On the other hand, with the eight-fold addition of F^- and AcO^- ions, the emission intensity gets significantly quenched with consequent red shift of emission maxima. Thus, the absorbance and luminescence behavior of the metalloreceptors toward the anions are in the same line. Photoluminescence titrations of receptors **1** and **2** with various anions have been carried out in the same way as was already described for spectrophotometric measurements. The lowest-energy emission maxima in both compounds get gradually red-shifted with consequent quenching with increasing anion concentration, indicating a lowering in the energy of the excited state and enhancement of nonradiative decay. In Figure 11, the effects of the incremental addition of AcO^- and F^- to **1** and **2**, respectively, are shown, and the inset shows quenching of the luminescence intensity versus the equivalents of anions added. Spectrofluorometric titrations of the sensors have also been carried out with a standard solution of TBAOH, and the observed spectral patterns (Figure S9, Supporting Information) follow trends similar to those seen with the incremental addition of the anionic guest. It is evident that the stronger bases and hydrogen-bonding acceptors such as AcO^- and F^- as well as OH^- completely quench the fluorescence of the metalloreceptors, implying that N−H protons of coordinated $H_2Imbzim^-$ are trapped by these anions. An almost complete quenching of the emission intensity by F^- and AcO^- over other anions makes the complexes selective fluorescent sensors.

(53) (a) Kang, S. O.; Powell, D.; Day, V. W.; Bowman-James, K. *Angew. Chem., Int. Ed.* **2006**, *45*, 7882. (b) Gunnlaugsson, T.; Kruger, P. E.; Jensen, P.; Tierney, J.; Ali, H. D. P.; Hussey, G. M. *J. Org. Chem.* **2005**, *70*, 10875. (c) Gunnlaugsson, T.; Kruger, P. E.; Jensen, P.; Pfeffer, F. M.; Hussey, G. M. *Tetrahedron Lett.* **2003**, *44*, 8909. (d) dos Santos, C. M. G.; Gunnlaugsson, T. *Dalton Trans.* **2009**, 4712. (e) Gomez, D. E.; Fabbrizzi, L.; Liccheli, M. *J. Org. Chem.* **2005**, *70*, 5717. (f) Amendola, V.; Boiocchi, D.; Colasson, B.; Fabbrizzi, L. *Inorg. Chem.* **2006**, *45*, 6138.

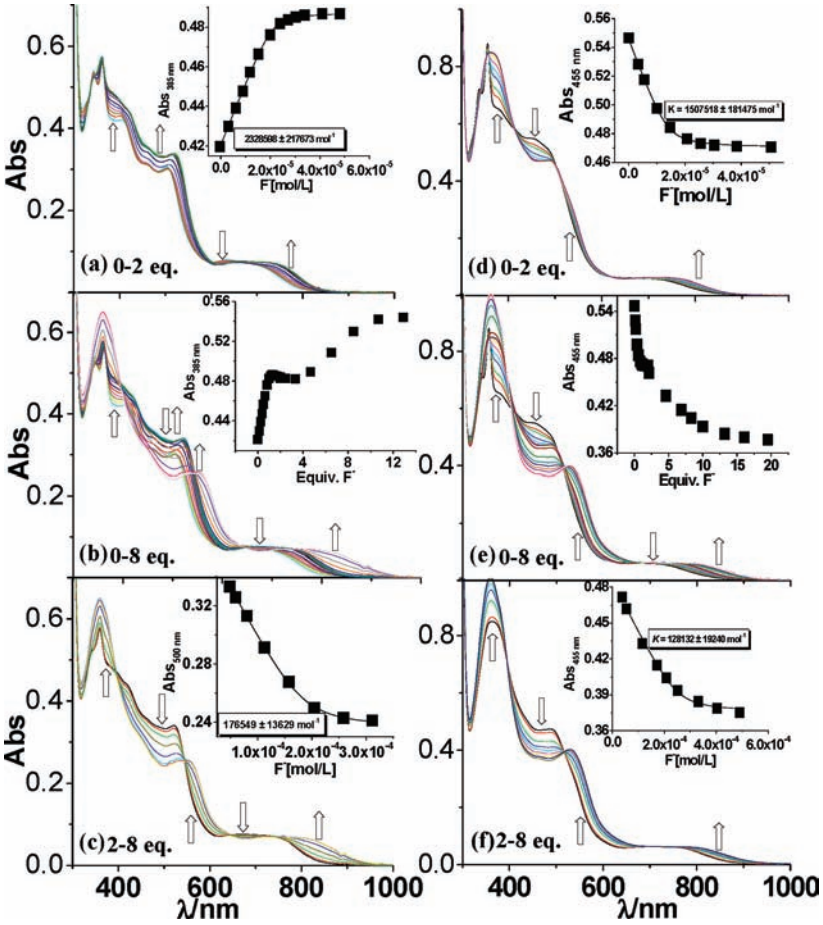

Figure 9. Changes in UV−vis spectra of receptors **1** (a−c) and **2** (d−f) in acetonitrile upon the addition of the F^- ion. The inset shows the fit of the experimental absorbance data to a 1:1 binding profile.

Table 6. Equilibrium/Binding Constants[a] (K, M^{-1}) for the Complexes toward Various Anions at 298 K

	1		**2**	
anion	$K_1 \times 10^6$	$K_2 \times 10^5$	$K_1 \times 10^6$	$K_2 \times 10^5$
		Absorption		
F^-	2.3 ± 0.21	1.8 ± 0.13	1.5 ± 0.18	1.3 ± 0.19
AcO^-	2.2 ± 0.14	1.6 ± 0.23	2.3 ± 0.32	1.8 ± 0.26
OH^-	2.3 ± 0.15	1.6 ± 0.12	2.0 ± 0.26	1.7 ± 0.19
		Emission		
F^-	1.5 ± 0.14	NA[b]	1.6 ± 0.15	NA[b]
AcO^-	1.6 ± 0.15	NA[b]	1.5 ± 0.22	NA[b]
OH^-	1.9 ± 0.14	NA[b]	1.5 ± 0.12	NA[b]

[a] *tert*-Butyl salts of the respective anions were used for the studies. [b] Not applicable.

Changes in the Electrochemical Behavior of the Receptors upon Interaction with Anions. The electrochemical anion recognition and sensing of the receptors in acetonitrile as a function of the different anions have been examined by using CV and SWV. The incremental addition of F^- and AcO^- ions to a solution of the receptors resulted in a negative shift of both the first ($E_{1/2}{}^1$) and second ($E_{1/2}{}^2$) oxidation potentials of **1** and **2**. As shown in Figure 12a,c, with the progressive addition of F^- to **2**, the current heights of the redox couples observed at 0.53 ($E_{1/2}{}^1$) and 1.07 V ($E_{1/2}{}^2$) gradually diminish and at their expense two new couples that appear at 0.32 ($E_{1/2}{}^1$) and 0.93 V ($E_{1/2}{}^2$), respectively, grow in the current heights. As the receptor−anion ratio reaches 1:1, the couples at 0.53 and 1.07 V are completely replaced by the 0.32 and 0.93 V couples, respectively, indicating that the shifts of $E_{1/2}{}^1$ and $E_{1/2}{}^2$ are −0.21 and −0.14 V, respectively. Upon further addition of the F^- ion to the solution of **2**, the second oxidation peak ($E_{1/2}{}^2$) at 0.93 V continues to shift in the lower potential region and finally becomes $E_{1/2}{}^2$ = 0.64 V with the addition of 3 equiv of the F^- ion, although the potential of the first couple $E_{1/2}{}^1$ remains constant at 0.32 V. The changes in the current heights for the redox couples with the variation of the concentration of added F^- ion are shown in Figure 12b,d. In the case of **1**, similar electrochemical responses are observed (Figure S10a,c, Supporting Information) upon the addition of 1 equiv of F^-, with the difference that the second oxidation potential ($E_{1/2}{}^2$) initially observed at 0.55 V is shifted to 0.15 V, keeping $E_{1/2}{}^1$ at 0.42 V unchanged. However, beyond 1 equiv, contrary to that of **2**, the current heights associated with the second oxidation at 0.42 V gradually decrease and diminished completely, and at its expense, the current intensity at 0.15 V continued to increase until both of the oxidation peaks due to Os^{II} centers coalesced at the same potential (0.15 V). The electrochemical behavior observed with AcO^- as the guest anion is almost identical with that of F^- for both **1** and **2**. In contrast to F^- and AcO^-, no noticeable changes occur in electrochemical

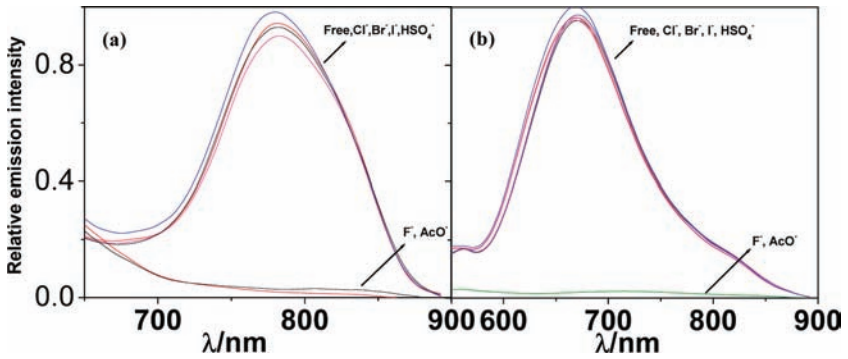

Figure 10. Changes in photoluminescence spectra of receptors **1** (a) in dichloromethane and **2** (b) in acetonitrile upon the addition of different anions as TBA salts.

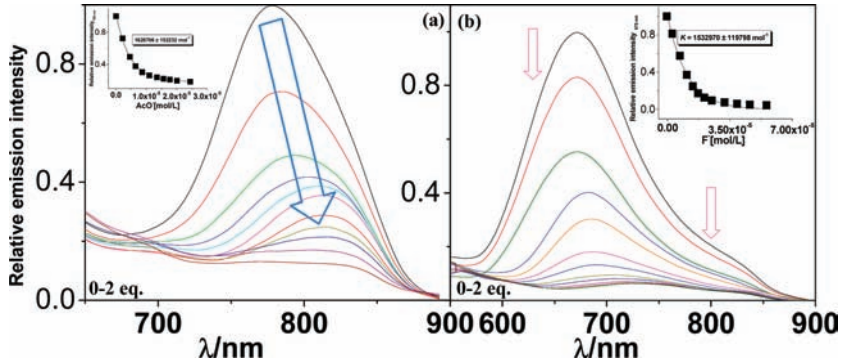

Figure 11. Changes in photoluminescence intensity of receptor **1** (a) in dichloromethane and **2** (b) in acetonitrile upon addition of AcO^- and F^- ions, respectively. Inset shows the fit of the experimental emission data to a 1:1 binding profile.

responses for **1** and **2** in the presence of a large excess of Cl^- and HSO_4^-.

As compared to complexes $\mathbf{1}^{3+}$, $\mathbf{2}^{3+}$, and related diruthenium $[Ru^{II}Ru^{II}]^{3+}$, the redox potentials of corresponding anion-bound forms are substantially shifted to less positive potentials. The lowering of the $E_{1/2}$ values upon the addition of anions is correlated with the spectral red shifts that occur for the MLCT bands. For example, in the case of $Ru^{II}Os^{II}$, anion-induced deprotonation is accompanied by lowering of the redox potentials $\Delta E_{1/2}(1)$ and $\Delta E_{1/2}(2)$ by 210 and 430 mV, respectively, while diminution of the two ^{1}MLCT band energies ($\Delta\nu$) occurs by about 1540 cm^{-1} (490 → 530 nm) and 2966 cm^{-1} (458 → 530 nm). Similarly, for $Ru^{II}Ru^{II}$, the corresponding lowering of the redox potentials occurs by 260 mV [$\Delta E_{1/2}(1)$], keeping $\Delta E_{1/2}(2)$ unchanged and diminution of the MLCT band energies ($\Delta\nu$) by ca. 690 and 866 cm^{-1}. However, in the case of $Os^{II}Os^{II}$, two successive oxidation peaks at 0.42 and 0.55 V merge to a single peak at 0.15 V upon deprotonation. In this case, lowering of the redox potentials occurs by 400 mV and diminution of the MLCT band energies by ca. 1375 cm^{-1} (507 → 545 nm) and 3390 cm^{-1} (460 → 545 nm).

It is relevant to compare the equilibrium constant K_c for the comproportionation reaction (eq 11) for the homobimetallic ruthenium(II) and osmium(II) complexes. The value of K_c at 298 K is evaluated by using eq 12.[54]

$$M^{II}M^{II} + M^{III}M^{III} \rightleftharpoons 2M^{II}M^{III} \tag{11}$$

$$K_c = 10^{16.92[E_{1/2}(2) - E_{1/2}(1)]} = 10^{16.92\Delta E_{1/2}(V)} \tag{12}$$

When there is no interaction between the two redox states (class I system), the value of K_c is equal to 4 because of the statistical effect only. On the other hand, a value of K_c as high as 2×10^{24} has been reported for a fully valence-delocalized (class III) system.[55] However, for a large number of diruthenium(II) and diosmium(II) complexes, the values of K_c have been found to range between 10^2 and 10^8.[54] Importantly, several studies have pointed out that specifying mixed-valence systems in the Robin and Day classification scheme[56] on the basis of their K_c values alone may lead to the wrong information.[57,58] The values of $\Delta E_{1/2}$ and K_c listed in Table 5 indicate that the K_c value of $[Ru^{II}Ru^{II}]^{3+}$ is greater than that of $[Os^{II}Os^{II}]^{3+}$. It is interesting to note that the value of K_c for the anion-induced deprotonated form $[Ru^{II}Ru^{II}]^{+}$ (1.3×10^7) is about 4 orders of magnitude greater than that for $[Ru^{II}Ru^{II}]^{3+}$.[19a] By contrast, the K_c value of $[Os^{II}Os^{II}]^{+}$ is very much less because we have seen that two oxidation peaks in $[Os^{II}Os^{II}]^{3+}$ coalesce into a single peak upon deprotonation.

(54) (a) Crutchley, R. J. *Adv. Inorg. Chem.* **1994**, *41*, 273. (b) Evans, C. E. B.; Naklicki, M. L.; Rezvani, A. R.; White, C. A.; Kondratriev, V. V.; Crutchley, R. J. *J. Am. Chem. Soc.* **1998**, *120*, 13096.

(55) Woldarezyr, A.; Doyle, G. A.; Maher, J. P.; McCleverty, J. A.; Ward, M. D. *Chem. Commun.* **1997**, 769.
(56) Robin, M. B.; Day, P. *Adv. Inorg. Chem. Radiochem.* **1968**, *10*, 247.
(57) Kaim, W.; Lahiri, G. K. *Angew. Chem., Int. Ed.* **2007**, *46*, 1778.
(58) Launy, J.-P. *Chem. Soc. Rev.* **2001**, *30*, 386.

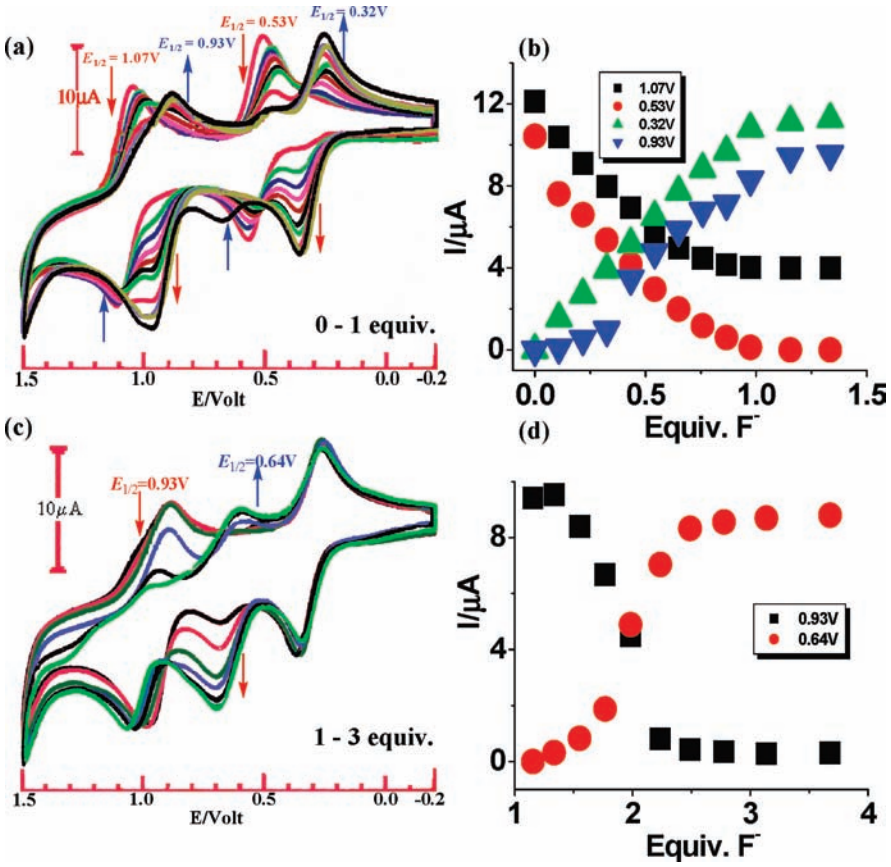

Figure 12. CVs of receptor **2** (a and c) obtained upon the incremental addition of TBAF to its acetonitrile solution (1.0×10^{-3} M). The changes in the current intensities as a function of the equivalents of the F^- ion added are shown in parts b and d.

Nature of Receptor−Anion Interaction. The observations made above from ^{1}H NMR and spectrophotometric, luminescence, and electrochemical measurements unequivocally suggest that F^- and AcO^- anions interact strongly with the metalloreceptors **1** and **2**; albeit such interaction is either very weak or absent for other anions (Cl^-, Br^-, I^-, and HSO_4^-). The close resemblance of both absorption and emission spectral patterns of the receptors in the presence of OH^- to those in the presence of F^- and AcO^- ions suggests the presence of two successive anion-induced deprotonation steps, leading to the formation of $[(bpy)_2M(HImbzim)M'(bpy)_2]^{2+}$ and $[(bpy)_2M(Imbzim)M'(bpy)_2]^{+}$ species. Fitting the overall titration data by assuming the existence of two sets of equilibria gives the association constants summarized in Table 6. It may be noted that the equilibrium constants of the metal complexes with the anions are grossly of 6 orders of magnitude. Comparable values of the association constants of the related ruthenium(II) complexes have been previously reported.[19a] It is of interest to note that the equilibrium constants of the metal complexes with the anions are substantially enhanced (2 orders of magnitude) relative to that of the ligand H_3Imbzim itself. Clearly, metal coordination leads to augmentation of the acidity of the imidazole NH protons.

In the literature, several functionalized derivatives of the Ru^{II}bpy systems have been reported as anion sensors where responses to changes of the electrochemical and luminescence signals have been investigated.[2−4] Ruthenium(II) complexes containing the Ru^{II}bpy moiety as a chromophore and the bis(imidazole) ligand as the binding site have been found to exhibit colorimetric sensing of anions. The important feature for such a construction is that the chelating coordination enforces the syn conformation of two NH protons in imidazole ligands.[3,20] We note that, although Ru^{II}-containing anion sensors are quite abundant now, studies with $Ru^{II}Ru^{II}$-, $Os^{II}Os^{II}$-, and $Os^{II}Ru^{II}$-containing systems similar to those reported by us are still confined to very few cases.

Conclusion

In conclusion, we have successfully designed redox-active and photoactive homobimetallic osmium(II) and heterometallic ruthenium(II)−osmium(II) bipyridyl complexes containing the H_3Imbzim ligand as the receptor unit, which are capable of multichannel recognition and sensing of a selective anionic guest. The solid-state X-ray crystal structures of both complexes **1** and **2** have shown that the two NH groups adopt a cis arrangement, and this pair of externally directed NH protons of $H_2Imbzim^-$ has been used for the formation of an adduct with anionic guests. The absorption spectra, luminescence properties, and electrochemical behavior of both complexes have been thoroughly investigated. In the heterobimetallic complex, photoinduced energy transfer from the Ru^{II}-based moiety to the Os^{II}-based luminescent ^{3}MLCT levels takes place with a rate constant of 6.1×10^7 s^{-1} at room temperature. The anion-sensing properties of the metalloreceptors have been confirmed by absorption, emission, and ^{1}H NMR spectroscopic techniques. Sensing studies suggest the presence of two successive anion-induced deprotonation steps, leading to the formation of $[(bpy)_2M(HImbzim)M'(bpy)_2]^{2+}$ and

$[(bpy)_2M(Imbzim)M'(bpy)_2]^+$ species. This event is signaled by the development of intense and beautiful colors visible with the naked eye. Electrochemical investigations have shown that these receptors electrochemically sense F^- and AcO^- anions via significant cathodic shifts of the respective M^{II}/M^{III} redox couples. Photophysical studies demonstrated a total quenching of the emission intensity resulting from the addition of F^- and AcO^- to the solutions of the receptors. It is gratifying to note that **1** and **2** behave as triple-channel metalloreceptors.

Acknowledgment. Financial assistance received from the Department of Science and Technology, New Delhi India (Grant SR/S1/IC-06/2006), and the Council of Scientific and Industrial Research, New Delhi, India (Grant 01(2084)/06/EMR-II), is gratefully acknowledged. Thanks are due to the Department of Inorganic Chemistry of Indian Association for the Cultivation of Science, Kolkata, India, for single-crystal X-ray data. D.S., S.D., and D.M. thank CSIR for their fellowship.

Supporting Information Available: X-ray crystallographic files in CIF format for compounds **1** and **2** and Figures S1−S11. This material is available free of charge via the Internet at http://pubs.acs.org.